Master's thesis

NTNU
Norwegian University of Science and Technology
Faculty of Engineering
Department of Civil and Environmental Engineering

Jonas Økern

Mechanical Characterization of Quarry Fines for Road Frost Protection Layers

Master's thesis in Civil and Environmental Engineering

June 2020

NTNU
Norwegian University of Science and Technology

Jonas Økern

Mechanical Characterization of Quarry Fines for Road Frost Protection Layers

Master's thesis in Civil and Environmental Engineering
June 2020

Norwegian University of Science and Technology
Faculty of Engineering
Department of Civil and Environmental Engineering

NTNU
Kunnskap for en bedre verden

Preface

The efforts of Professor Inge Hoff and postdoc Diego Barbieri in guiding this project are greatly appreciated. The latter is also recognized for providing inordinate amounts of baked goods and for rocking a wizard's lightning bolt carved into his hair. The lab personnel and their patience regarding my staggering lack of some basic human practical skills must also be acknowledged. (I am now capable of naming several new tools without resorting to the phrase "thingy".) I am very grateful for the financial support and guidance from Asplan Viak. Finally, I would like to thank everyone at the Public Roads Administration who helped me, though a sudden pandemic made our intended collaboration impossible.

When the Norwegian constitution was established, the public representatives swore to remain "compliant and steadfast until the fall of the Dovre-mountains". They probably equated that timeframe with forever. But as every geologist knows; everything is reduced to dust in the end. All we can do as people and engineers is postpone the inevitable deterioration of all things. So here is my little contribution to the anti-dust campaign.

Also, I suspect I will be searching the inaccessible crevices of my skin for master's-thesis fine particles gone astray until I kick the bucket.

Trondheim, June, 2020
Jonas Økern

Contents

Mechanical Characterization of Quarry Fines for Road Frost Protection Layers

Jonas Økern

Abstract

The purpose of this research is to assess the mechanical properties of quarry fines, to evaluate the potential of utilizing the material in road frost protection layers. Quarry fines are underutilized surplus materials, meaning new applications should be developed. For this purpose, the resilient modulus of two 0/4 mm aggregates was determined using repeated load triaxial tests. Then, the load-response of untreated and lignosulphonate stabilized quarry fines frost protection layers was simulated through numerical modeling using the triaxial test data.

12 repeated load triaxial tests were performed with the multistage procedure at low stress levels. The quarry fines were tested untreated at 1 % and 7 % water content, as well as with 1.2 % cured lignosulphonate, to investigate the potential of additive stabilization.

The resilient modulus of the untreated fines was approximately 100-300 MPa for sequence 1 stresses: σ_d of 20-120 kPa and $\sigma_t = 20$ kPa. The additive treatment improved stiffness by a large, but inconsistent magnitude; with a stabilized resilient modulus of roughly 400-10000 MPa for the same sequence 1 stresses.

The best fit for the $k-\theta$ and a universal octahedral resilient modulus model was established using regression analyses. The universal model fit achieved $R^2 > 0.90$ for most of the untreated tests. While post stabilization, the data-scatter was significant, resulting in $R^2 \epsilon [0.15, 0.73]$.

The lignosulphonate additive improved the resistance to permanent deformation in the quarry fines substantially. Specifically, the accumulated axial plastic strain in the triaxial tests was approximately halved through stabilization. Also, the triaxial load step strain rates showed considerably more elastic than plastic behavior with the additive treatment. From the triaxial test results, a good fit for a time-hardened permanent deformation model was determined.

Stabilized and untreated quarry fines road frost protection layers were simulated in multiple layer linear elastic and finite element analyses, using respectively *ERAPave* and *COMSOL Multiphysics*. The simulations accounted for non-linear elasticity through the triaxial test stress-dependent regression models.

Under tandem rig loads, the calculated load response indicates that the mechanical properties of stabilized quarry fines are sufficient for use as road frost protection layers. Further, the performance modeling supports this conclusion; showing that road frost protection layers with lignosulphonate treated quarry fines will likely not develop excessive permanent deformation when exposed to medium traffic.

Keywords: repeated load triaxial tests (RLTTs), quarry fines stabilization, road frost protection layers, mechanistic-empirical design, aggregate material characterization

1 Introduction

The objective of this thesis is to perform a mechanical classification of quarry fines. Therefore, section 1 introduces the material and related civil engineering challenges.

1.1 Quarry fines and the Norwegian aggregate industry

Quarry fines are a surplus material generated by the blasting, transport and crushing procedures of aggregate production. Significant volumes of fine particles are also generated during highway - and tunnel-construction, through drilling and blasting operations, and especially when using tunnel boring machines [1]. Due to documented poor material properties, application of these

materials is currently strictly regulated by the relevant technical standards [2, 3, 4, 5]. Thus, the material is available at low prices and in large quantities at most quarries.

The Norwegian Geological Survey has registered more than 10 000 deposits for virgin sand and gravel, and hard rock aggregate across the country [6, 7]. From the licensed production sites, 94 million tons of aggregate materials were sold in 2018, which equated to a turnover of 6 757 million NOK [8]. Further, at least 30 million additional tons were extracted from hard rock during infrastructure construction [8, 9].

The geographical distribution of deposits is not equivalent to construction industry demand regarding neither quality nor quantity [10]. Consequently, the Directorate of Mining reports an average annual transport length of 18 km/tons, and that unsold surplus material constituted 10-25 % of the production between 2010-2018 [8]. The ratio of particles < 4 mm among this total surplus was not reported, but is likely at least 30-40 % [11, 12].

The virgin sand and gravel aggregate deposits in Norway are frequently of non-renewable glaciofluvial origin [12], although some key fluvial and moraine deposits also exist [13]. The available high-quality deposits may be subject to political conflicts of interests [7], like concerns for dust and noise pollution, alternate use as groundwater aquifers or plot for construction sites. These issues all lead to increased pressure for utilizing manufactured crushed aggregates, which now comprise around 88 % of the annual aggregate production in Norway [8].

Finding applications for quarry fines surplus is beneficial for the aggregate- and construction industry, and for Norwegian society in general. Considering, such applications may prevent unnecessary landfill usage, alleviate the use of valuable non-renewable aggregate materials, reduce material transport distances and lower construction costs.

1.2 Quarry fines properties and uses

The Norwegian geotechnical classification of soils defines the category of a single soil particle based on the diameter, d_i [14]. Classically, fines would be the cohesive soils: clay ($d_{clay} \leq 0.002$ mm) and silt (0.002 mm$< d_{silt} \leq 0.063$ mm) [14]. The notation d/D may be used to denote the upper and lower bounds for the particle sizes included in a mix. For fines, aggregate trade denominations operate with fractions like 0/2 or 0/4 mm, often collectively referred to as sand or manufactured sand.

The quarry fines fractions are utilized in a variety of engineering applications. Firstly, Norwegian highways are often constructed of unbound granular materials (UGMs) in the base, the subbase and the frost protection layers (FPLs) [15, 16]. Nevertheless, the unbound base and subbase are limited to $\leq$ 3-7 % of the particles passing a 0.063 mm sieve [2]. Similarly, concrete employs fines-rich fractions like 0/8 mm [5], but too high fines content will increase the water demand and negatively impact the workability of the recipe [10]. Hence, concrete for bridges and ferry docks only allows 1.5 % or 10 % of aggregate <0.063 mm [17]. Finally, railway ballast is highly uniformly graded at 31.5/63 mm, and contains $\leq$ 0.6 % material < 0.5 mm [3].

1.3 Norwegian highway design

To avoid excessive frost heave, Norwegian superstructures subjected to >1500 AADT are designed to prevent the freezing front from penetrating frost susceptible subgrades, for a design winter with a return period or 10 or 100 years depending on traffic [2].

The structural design is performed through the index-method in the Norwegian Public Roads Administrations (NPRAs) *Handbook N200* [2]. There, materials are assigned E-modulus based load distribution factors ($a_{material}$), relative to standardized gravel with $a = 1.0$. The bearing capacity is evaluated by multiplying the load distribution factor with the layer thickness (t). This product is summed up: $Index = \sum_{i=1}^{n} a_i \cdot t_i$, for n materials in the structure.

This empirical design system is unfit to evaluate new or alternate materials, such as quarry fines. However, the NPRA is adopting mechanistic-empirical (ME) design. Namely, developing

and implementing the Swedish National Road and Transport Research Institute's software *ERAPave*. The software uses the multiple layer linear elastic method (MLLEM) to simulate load response and performance, rendering it capable of evaluating the structural viability of quarry fines as road FPLs. Thus, it will be adopted along with the finite element method (FEM) in *COMSOL Multiphysics* for the response modeling of quarry fines in this research.

1.4 Research objective

Recent investigations into the basic properties of quarry fines, with gradation and frost heave tests, indicate that the material is frost susceptible [18, 19]. This demonstrates that stabilizing additives may be necessary for the use of quarry fines in infrastructure exposed to seasonal frost.

A rational response to the quarry fines surplus issue is improving the material quality. For instance, by implementing inter-particle crushing, using a shaft impactor crushing stage [20]. The inter-particle crushing creates a more beneficial grain shape, especially for concrete [20]. Moreover, sorting particles by using wind sieving allows for much preciser gradation control [20]. The combination of these technologies creates a superior product, referred to as manufactured sand, and may be a partial solution to the surplus issue. Nonetheless, even industrywide adoption of manufactured sand methodology may not be enough to nullify the entire quarry fines surplus.

At road FPL depth, the traffic load is considerably distributed. Therefore, the mechanical requirements of the FPL are not particularly strict. Essentially, a cheap, non-frost susceptible material, of reasonable mechanical quality is required in large volumes. The potential for utilizing stabilized quarry fines here seems significant. Accordingly, the basic research objective of this thesis is defined: *The mechanical properties of untreated and lignosulphonate stabilized quarry fines surplus, and their load response in road FPLs must be determined.*

2 Mechanical properties of unbound granular materials

Quarry fines may be categorized as UGMs, which can be idealized as more or less homogeneous friction-soils. Meaning, the shear-strength in the material is caused by friction and interlocking in the contact surfaces of the soil particle matrix. Further, the deformation properties can be characterized as elastoplastic; the total axial strain (ϵ_{tot}) for a pulse of compressing stress will consist of an axial elastic/reversible (ϵ_r) and an axial plastic/irreversible component (ϵ_p): $\epsilon_{tot} = \epsilon_{elastic} + \epsilon_{plastic} = \epsilon_r + \epsilon_p$. This concept is illustrated on Figure 1.

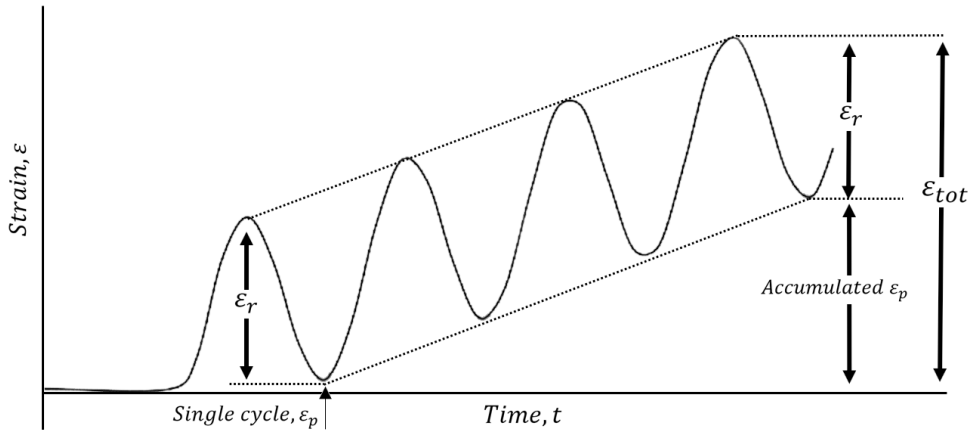

Figure 1: The elastoplastic deformation properties of UGMs.

ϵ_r is reclaimed at stress relaxation, while ϵ_p is accumulated with increasing load cycles and time (accumulated plastic strain may be denoted $\hat{\epsilon_p}$). ϵ_p is exaggerated in the figure to illustrate the principle, usually $\epsilon_p \ll \epsilon_r$ for normal traffic loads.

Extensive research shows that both the elastic deformation (ED) [21] and the permanent deformation (PD) [22] are non-linearly dependent on the stress level. Of note, the ED causes tensile strains strongly associated with surface fatigue cracking [23]. Meanwhile, rutting from PD in UGMs constitutes an important damage mechanism, especially on low traffic roads with thin asphalt layers [24]. Thus, both ED and PD properties are necessary for a complete mechanical classification of quarry fines.

Of note, for UGMs, a total stress analysis is usually performed due to assumed coarse aggregates providing drained conditions. Depending on the permeability of the quarry fines, and the drainage boundary conditions, this simplification may not be accurate.

2.1 Elastic deformation and resilient modulus

Load response modeling of quarry fines will require the elastic stiffness. UGMs are characterized by having a stress-dependent non-linear elastic stiffness [21]. The term resilient modulus (M_r) may be used in place of E-modulus when accounting for the non-linear behavior.

Mechanically, M_r expresses the ratio between elastic axial strain (ϵ_a) and dynamic deviator stress (σ_d): $M_r = \Delta\sigma_{dynamic,\ deviator}/\Delta\epsilon_{axial,\ elastic} = \Delta\sigma_d/\Delta\epsilon_a$. Graphically, this is equivalent to the slope of the elastic section of the curve in a stress-strain work diagram, based on a repeated load triaxial test (RLTT) stress situation, as shown in Figure 2.

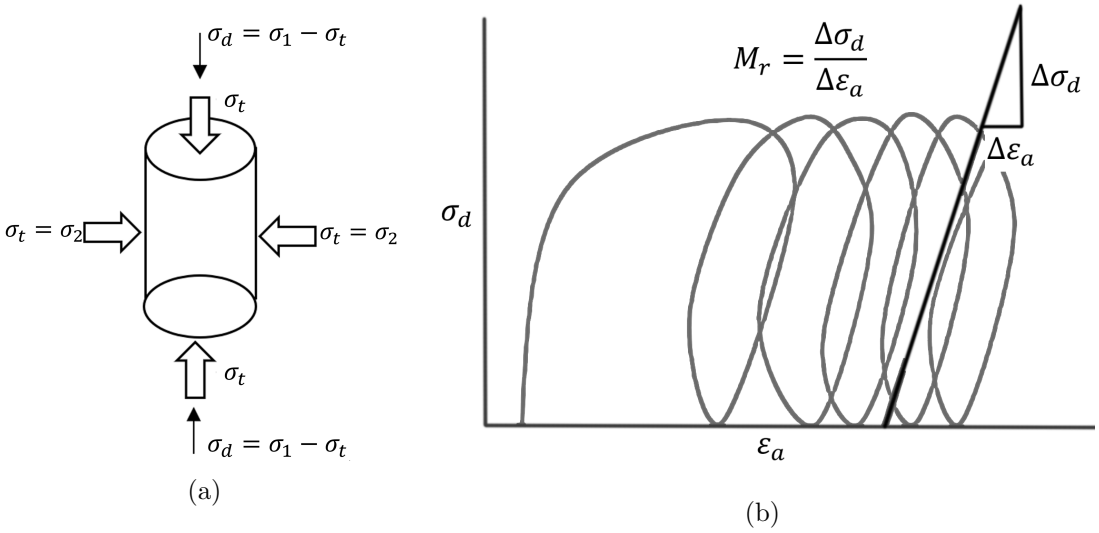

Figure 2: **(a)** RLTT stress situation, with stresses simplified as vector arrows. **(b)** Definition of resilient modulus from stress-strain diagram based on UGM RLTTs.

Here, $\Delta\sigma_{dynamic,\ deviator} = \sigma_1 - \sigma_t$, is the deviatoric stress. For σ_1, σ_2 and σ_3 as the largest, intermediate and smallest principal stresses. Meanwhile, $\Delta\epsilon_{axial,\ elastic}$ is the recoverable axial strain upon stress relaxation. Effectively, the RLTT may be biaxial, with constant hydrostatic stress of $\sigma_t = \sigma_2 = \sigma_3$.

Comprehensive RLT testing shows that the stress level is the most important factor for the resilient modulus [21]. However, a larger scientific literature review reveals that density, gradation parameters, fines content, aggregate type, grain shape, water content and stress history also have influence [25].

2.2 Material models for resilient modulus

To simulate the load response of quarry fines FPLs, a material model for resilient modulus is needed. There exists several applicable non-linear models [25, 26], many of which have been compared in other research [27].

Primarily, the models relate M_r to independent variables: deviatoric stress (σ_d), smallest principal stress (σ_3), or the sum of principal stresses (bulk stress, $\theta = \sigma_1 + \sigma_2 + \sigma_3$).

This research investigates 2 resilient modulus models. Firstly, the $k-\theta$ model [21] is used for the FEM in *COMSOL Multiphysics*. Secondly, the MLLEM *ERAPave* ME-design software has implemented a universal model recommended by the American *Mechanistic-Empirical Design Guide* (*MEPDG*) [28, 29].

The $k-\theta$ model

A straightforward model [21] relates the resilient modulus (M_r) to independent variable bulk stress (θ), with two regression coefficients (k_1 and k_2), for reference pressure $\sigma_a = 100$ kPa:

$$M_r = k_1 \cdot \sigma_a \cdot (\frac{\theta}{\sigma_a})^{k_2} \tag{1}$$

The universal model

A more comprehensive model was proposed by Uzan and Witczak [30], generalizing a model by Uzan [26] into 3D. One of the widely adopted [24, 27, 31, 32] *MEPDG* versions [28] of this concept is utilized here. The octahedral shear stress (τ_{oct}) is accounted for along with the bulk stress (θ), requiring 3 regression coefficients ($k_1 - k_3$):

$$M_r = k_1 \cdot \sigma_a \cdot (\frac{\theta}{\sigma_a})^{k_2} \cdot (\frac{\tau_{oct}}{\sigma_a} + 1)^{k_3} \tag{2}$$

The regression parameters should fulfill $k_1 > 0$, $k_2 \geq 0$ and $k_3 \leq 0$. k_1 should always be > 0 to ensure $M_r > 0$. Additionally, M_r ought to increase for increasing bulk stress (θ), meaning k_2 should be > 0. Meanwhile, k_3 is related to the octahedral shear stress (τ_{oct}), therefore, it should be negative to account for shear softening effects [29]. The octahedral shear stress is defined based on the principal stresses (σ_1, σ_2 and σ_3) as:

$$\tau_{oct} = \frac{1}{3} \cdot \sqrt{(\sigma_1 - \sigma_2)^2 + (\sigma_2 - \sigma_3)^2 + (\sigma_1 - \sigma_3)^2} \tag{3}$$

2.3 Permanent deformation in unbound granular materials

Based on RLTT data, the development of PD in UGMs can be sorted into 3 categories [33, 34], as depicted in Figure 3: *elastic*, *elastoplastic* and *failure/plastic*.

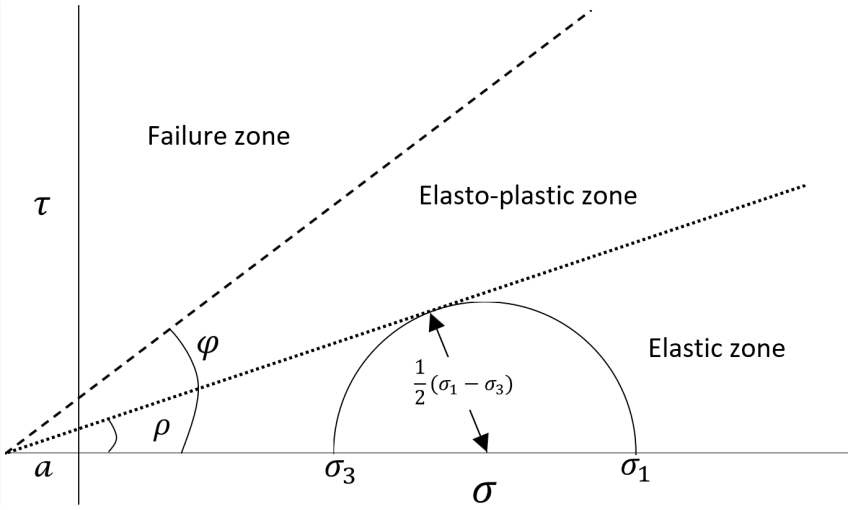

Figure 3: $\tau - \sigma$ plot with mobilized shear strength, angle of friction and elastoplastic categories.

σ_1, σ_2 and σ_3 remain the smallest, intermediate and largest principal stress, while maximum shear stress is equivalent to the radius in the Mohr-circle: $\tau_{max} = \frac{1}{2} \cdot (\sigma_1 - \sigma_3)$. The most important factor for the development of PD in UGMs may be mobilized shear strength (ρ) [35]:

$$sin(\rho) = \frac{\sigma_1 - \sigma_3}{\sigma_1 + \sigma_3 + 2a} \tag{4}$$

Here a is the apparent attraction in the material. When all RLTT loads steps are categorized, the results can be presented in a $\sigma_d - \sigma_3$ plot with the Coloumb criterion for elastic- and failure-line:

$$\sigma_d = \frac{2 \cdot sin(\rho) \cdot (\sigma_3 + a)}{1 - sin(\rho)} \tag{5}$$

The determination of quarry fines PD behavior, will in this research be performed according to strain per cycle (strain-rate, $\epsilon^{'}$). The category criterion based on the average vertical strain-rate for the last 5000 cycles in a RLTT load step are then [36]:

- Elastic (category A): $\epsilon_p^{'} < 2.5 \cdot 10^{-8}$
- Elasto-plastic (category B): $2.5 \cdot 10^{-8} < \epsilon_p^{'} < 1.0 \cdot 10^{-7}$
- Plastic/failure (category C): $1.0 \cdot 10^{-7} < \epsilon_p^{'}$

Previous RLTT experiments indicate that open-graded materials are weaker against PD than well graded, and that development of PD seems highly linked to stress-history and the degree of compaction [35, 37]. Although, a large literature review reveals that the dry density, degree of saturation, mineralogy, stress level and the fines content all influence the PD in UGMs [22].

2.4 Performance models for rutting in unbound granular materials

A large number of PD-models for UGMs exists [22]. The models typically relate the accumulated plastic strain ($\hat{\epsilon}_p$) to material parameters, number of applied load cycles (N) and stress levels.

The available PD models have been evaluated for Nordic conditions [38, 39], and 3 rutting performance models for UGMs were implemented in *ERAPave* [40, 41, 42]. Out of which a new version (unpublished) of the Rahman and Erlingsson model [42] will be utilized for characterizing the quarry fines in this research.

The Rahman, Erlingsson and Ahmed *ERAPave* rutting model

Rahman and Erlingsson present a rutting model for accumulated plastic strain ($\hat{\epsilon}_p$) as a function of applied load cycles (N) and the stress situation (S_f) [42]. The updated version of the model (unpublished) replaces stresses with the resilient strain (ϵ_r):

$$\hat{\epsilon}_p(N) = a \cdot N^{b \cdot \epsilon_r} \cdot \epsilon_r \tag{6}$$

Here, the regression parameters should be restricted as $0 < a$ and $100 < b < 1000$. The UGM PD-models are often based on only 1 stress path from an RLTT. However, it is desirable to account for stress-history in the modeling effort. For this purpose, multiple stress paths from a Multi-Stage (MS) triaxial test can improve the model with time-hardening effects [42, 43]:

$$\hat{\epsilon}_{p_i}(N) = a \cdot (N - N_{i-1} + N_i^{eq})^{b(\epsilon_r)_i} \cdot (\epsilon_r)_i \tag{7}$$

Where: $\hat{\epsilon}_{p_i}$ is accumulated plastic strain at the end of stress path (N) number i. Moreover, N_i^{eq} is the equivalent number of load cycles, which give the same accumulated plastic strain at a given stress level, as what was accumulated up to stress path nr. $(i-1)$:

$$N_i^{eq} = [\frac{\hat{\epsilon}_{p_{i-1}}}{a(\epsilon_r)_i}]^{b^{-1}(\epsilon_r)_i^{-1}} \tag{8}$$

3 Test program

The mechanical properties of UGMs subjected to dynamic loads can be comprehensively assessed through a RLTT, making it the primary experimental tool for this research.

3.1 Quarry fines test materials

To account for some of the inherent variability of natural materials, 2 different 0/4 mm quarry fines aggregates were investigated: Material 1 (M1) and Material 2 (M2). Material M1 is a mafic intrusive igneous gabbro and M2 is a metamorphic gneiss.

As a part of larger (unpublished) research into quarry fines materials at NTNU, several supplementary tests of materials M1 and M2 have been completed in accordance with NPRA *Handbook R210* [44]: sieve and hydrometer grain size distribution (GSD) analyses (tests *R210-131* and *132*), pycnometer test for specific density (test *R210-122*) and falling cone test for liquid limit (test *R210-216*). Additionally, a methylene blue specific surface area (SSA) test was performed on the < 75 μm fraction using standard *ASTM C837* [45]. Relevant basic material information and supplementary test results are presented in Table 1.

Table 1: Supplementary data for quarry fines test materials M1 and M2.

Material	**Quarry**	**Region**	**Primary rock type**	**Specific density** $[kg/m^3]$	**% mass** $< 75\mu m$	**% mass** $< 63\mu m$	**Liquid limit**, w_L [%]	**Methylene blue** SSA $[m^2/g]$
M1	Vassfjell	Trøndelag	Gabbro	3020	12.7	-	27.3	6.60
M2	Lørenskog	Viken	Gneiss	2881	19.1	15	31.0	6.40

Based on the preliminary GSDs, M1 and M2 are moderately frost susceptible. Future frost heave tests of untreated and stabilized M1 and M2 material will examine this in detail.

3.2 Test program overview

Both M1 and M2 were tested in the RLTT untreated at 1 % and 7 % water content, to gauge moisture sensitivity. Tests were also performed with 1.2 % cured lignosulphonate, to study the effect of stabilizing agents. Consistently, 2 parallel tests were executed for every combination of test conditions, totaling 12 tests. An overview of the test program is given in Table 2.

Table 2: Overview of RLTT samples. Including water content and additive by weight percentage, as well as dry and wet density post compaction.

Test designation	**Water content**		**Lignosulphonate**	**Wet density**	**Dry density**
$[material\_sample]$	w_{prep}	w_{test}	**additive**	ρ_{wet} $[kg/m^3]$	ρ_{dry} $[kg/m^3]$
M1_01	7 %	7 %	-	2254	2104
M1_02	7 %	7 %	-	2237	2087
M1_03	7 %	0.6 %	1.2 %	2342	2185
M1_04	7 %	0.6 %	1.2 %	2348	2190
M1_05	1 %	1 %	-	2067	2046
M1_06	1 %	1 %	-	2157	2136
M2_01	7 %	7 %	-	2222	2074
M2_02	7 %	7 %	-	2230	2081
M2_03	7 %	1.2 %	1.2 %	2293	2140
M2_04	7 %	0.4 %	1.2 %	2303	2148
M2_05	1 %	1 %	-	2066	2046
M2_06	1 %	1 %	-	2041	2021

3.3 Triaxial testing procedure

The RLTT works by applying a normal dynamic deviator stress (σ_d) to a prepared test specimen under a set confining/triaxial pressure (σ_t), as shown in Figure 2a. The confining pressure was bi-axially hydrostatic ($\sigma_t = \sigma_2 = \sigma_3$), provided by water. While the deformations were measured using 3 horizontal (radial) and 2 vertical linear variable differential transformers (LVDTs).

The tests were performed using the a RLT rig at the NTNU Civil- and Environmental Engineering laboratory facility, having served several previous projects studying UGMs [35, 37, 46, 47]. The equipment and sample preparation procedure is shown in Figure 4.

Figure 4a shows an approximately 11 kg cylindrical quarry fines sample with diameter $D = 15$ cm and height $h = 30$ cm. The sample has been compacted in 5 equal layers into the sample casing, using a Kango 950X vibrohammer at full effect for 30 seconds per layer. Each layer was separately premixed and homogenized to the prescribed water and additive content. Next, Figure 4b shows how the quarry fines are pressed out of the casing into the latex membrane secured with O-rings. On Figure 4c, a secondary membrane is attached and the sample is installed in the triaxial apparatus with LVDTs. Finally, in Figure 4d the chamber containing the sample is sealed and pressurized with water, before the vertical hydraulic jack applies σ_d.

(a) (b) (c) (d)

Figure 4: Sample preparation procedure for the RLTT.

Multistage procedure (MSP) low-stress level (LSL) tests were performed in compliance with standard EN-13286-7 [48]. The MSP LSL method determines the maximum stress level that can be applied before an unacceptable permanent axial strain of 0.5 % occurs.

Stress paths, shown in Table 3, were applied cyclically in 5 sequences each divided into 6 steps. With 10 Hz frequency, a load step consists of 10 000 cycles (N). Thereafter, a new step begins with increased σ_d and constant σ_t for stress paths in the same sequence. If strain exceeds the threshold, remaining steps in the sequence are aborted, and the next sequence initiates.

Table 3: MSP LSL RLTT σ_t and max deviatoric stress ($\sigma_{d_{max}}$), where $\sigma_{d_{min}} = 0$ [48].

Sequence 1 [kPa]		**Sequence 2** [kPa]		**Sequence 3** [kPa]		**Sequence 4** [kPa]		**Sequence 5** [kPa]	
σ_t	$\sigma_{d_{max}}$	σ_t	$\sigma_{d_{max}}$	σ_t	$\sigma_{d_{max}}$	σ_t	$\sigma_{d_{max}}$	σ_t	$\sigma_{d_{max}}$
20	20	45	60	70	80	100	100	150	100
20	40	45	90	70	120	100	150	150	200
20	60	45	120	70	160	100	200	150	300
20	80	45	150	70	200	100	250	150	400
20	100	45	180	70	240	100	300	150	500
20	120	45	210	70	280	100	350	150	600

3.4 Stabilization procedure

The stabilizing agent utilized in the laboratory tests was a lignosulphonate derived from lignin, branded Dustex. The product is a non-corrosive organic polymer extracted from plant biomass and is declared to be non-toxic [49].

A dose of 2.5 % by mass Dustex was mixed with water and applied to each of the five layers of the sample, which were then homogenized pre-compaction. Dustex is premixed with 50 % by mass water, meaning the true mass ratio of lignosulphonate binder was approximately 1.25 %.

After compaction, the samples were cured by air in a heating chamber, at a temperature of $50-60^oC$, until the desired residual water content was achieved. The curing process, illustrated in Figure 5, of evaporating roughly 6 % water took about 48 hours under these conditions.

Figure 5a is a top down view of uncured and untreated M1 quarry fines compacted into a RLTT sample. Then, Figure 5b shows a partially cured sample being weighed to estimate the current water content. Finally, Figure 5c displays 3 stabilized and cured samples in storage.

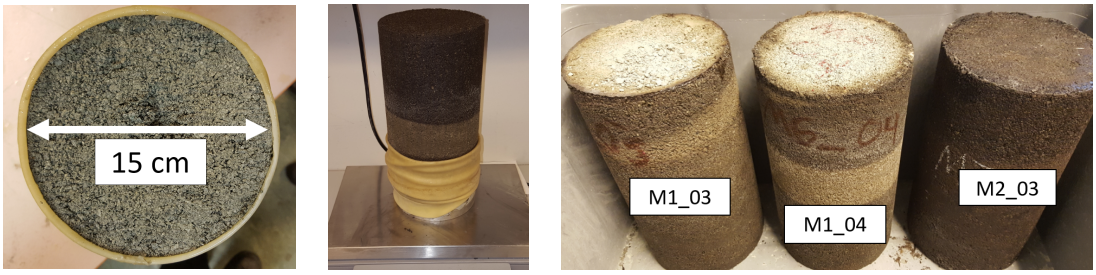

(a) (b) (c)

Figure 5: The curing process of additive stabilization with lignosulphonate.

4 Test results

Based on the 12 RLTTs performed, the ED and PD properties of the untreated and stabilized quarry fines were ascertained.

4.1 Resilient modulus assessment

The observed resilient modulus ranges for materials M1 and M2 are provided in Table 4 and Table 5 respectively. Further, the best fit for the $k-\theta$ [21] and the universal octahedral [28] resilient modulus models coefficients of regression are presented in Table 6.

Some extreme values were excluded from the data interpretation; for the untreated mixes M1_01 and M2_01, any instances of $M_r > 1000$ MPa were removed from the raw data. Moreover, sample M2_06 was entirely omitted from regression analyses due to severe PD after test sequence 2, which may have been caused by a membrane leak.

Table 4: Sequential (seq) minimum (min), arithmetic average (avg) and maximum (max) observed resilient modulus (M_r) for the RLT tests of material M1.

seq	**Untreated, w = 7 %**						**Stabilized, w = 0.6 %**						**Untreated, w = 1 %**					
	M1_01, M_r [MPa]			**M1_02**, M_r [MPa]			**M1_03**, M_r [MPa]			**M1_04**, M_r [MPa]			**M1_05**, M_r [MPa]			**M1_06**, M_r [MPa]		
	min	**avg**	**max**	**min**	**avg**	**max**	**min**	**avg**	**max**	**min**	**avg**	**max**	**min**	**avg**	**max**	**min**	**avg**	**max**
1	92	121	175	94	127	188	437	4107	9624	871	4437	10414	113	171	233	105	243	711
2	159	176	228	183	205	257	1299	3777	5314	3635	8032	13725	254	282	342	163	309	722
3	-	-	-	277	302	354	1354	3220	4193	1194	8111	12562	299	341	410	-	-	-
4	261	288	355	312	348	403	957	1844	3830	2602	11238	16484	334	395	479	-	-	-
5	355	385	478	412	441	514	1124	1423	2109	3239	7981	13738	423	504	616	-	-	-

Table 5: Sequential (seq) minimum (min), arithmetic average (avg) and maximum (max) observed resilient modulus (M_r) for the RLT tests of material M2.

seq	**Untreated, w = 7 %**						**Stabilized, w = 1.2 % and 0.4 %**						**Untreated, w = 1 %**					
	M2_01, M_r [MPa]			**M2_02**, M_r [MPa]			**M2_03**, M_r [MPa]			**M2_04**, M_r [MPa]			**M2_05**, M_r [MPa]			**M2_06**, M_r [MPa]		
	min	**avg**	**max**	**min**	**avg**	**max**	**min**	**avg**	**max**	**min**	**avg**	**max**	**min**	**avg**	**max**	**min**	**avg**	**max**
1	117	175	525	92	109	150	347	1026	2832	1229	3871	6910	139	214	299	143	176	293
2	-	-	-	418	540	801	289	429	957	3596	9355	16719	270	305	359	223	263	319
3	173	185	294	190	207	295	266	320	1167	6285	13679	22252	328	381	457	277	321	388
4	197	215	265	204	235	292	313	351	955	3566	17599	30671	417	475	566	417	475	566
5	225	253	373	266	308	392	423	501	2096	4988	17328	29582	520	591	704	429	506	629

Table 6: Regression coefficients for the $k-\theta$ [21] and the universal [28] M_r [MPa] models.

Sample	**Lignosulphonate additive**	**Water content**	**$k-\theta$ model**			**Universal model**			
			k_1	k_2	R^2	k_1	k_2	k_3	R^2
M1_01	-	7 %	1.0296	0.6598	0.95	1.0281	0.7854	-0.2966	0.96
M1_02	-	7 %	1.2119	0.6579	0.94	1.1702	0.8705	-0.4700	0.98
M1_03	1.2 %	0.6 %	39.669	-0.2696	0.15	37.770	-0.3807	0.3374	0.15
M1_04	1.2 %	0.6 %	47.947	0.4102	0.41	47.060	0.1288	0.6574	0.48
M1_05	-	1 %	1.6355	0.5633	0.97	1.6303	0.6285	-0.1428	0.98
M2_01	-	7 %	1.6948	0.1640	0.17	1.7445	0.1980	-0.1557	0.18
M2_02	-	7 %	1.7183	0.2918	0.17	1.7183	0.2918	0.0000	0.17
M2_03	1.2 %	1.2 %	11.494	-0.8414	0.61	12.996	-0.6463	-0.6972	0.62
M2_04	1.2 %	0.4 %	46.969	0.7492	0.72	47.230	0.6583	0.2008	0.73
M2_05	-	1 %	1.9455	0.5411	0.93	1.8956	0.6991	-0.3136	0.96
M2_06	-	1 %	1.6246	0.5871	0.92	1.5987	0.7062	-0.2421	0.94

Resilient modulus of untreated quarry fines

The untreated mixes of materials M1 and M2 display similar resilient behavior. Evidently, M1 is stiffer at higher stress levels and higher water content. Contrarily, M2 is stiffer for lower stress levels and lower water content. However, the differences are not reliable, and no decisive quality delineation is obvious from the limited data available.

Generally, the untreated stiffness of both M1 and M2 increased for increasing stress level; the average observed resilient modulus ($M_{r,\ avg}$) was raised by an average ratio of 37 % per RLT test sequence for M1 fines, and by 43 % for M2 fines. Further, the untreated M_r increased for decreasing water content; for M1, $M_{r,\ avg}$ was 29 % higher at w = 1 % than at w = 7 %. Likewise, M2 displayed 55 % higher $M_{r,\ avg}$ at w = 1 % than at w = 7 %. Figure 6 and 7 show the observed M_r for M1 and M2 respectively, as a function the load cycles (N).

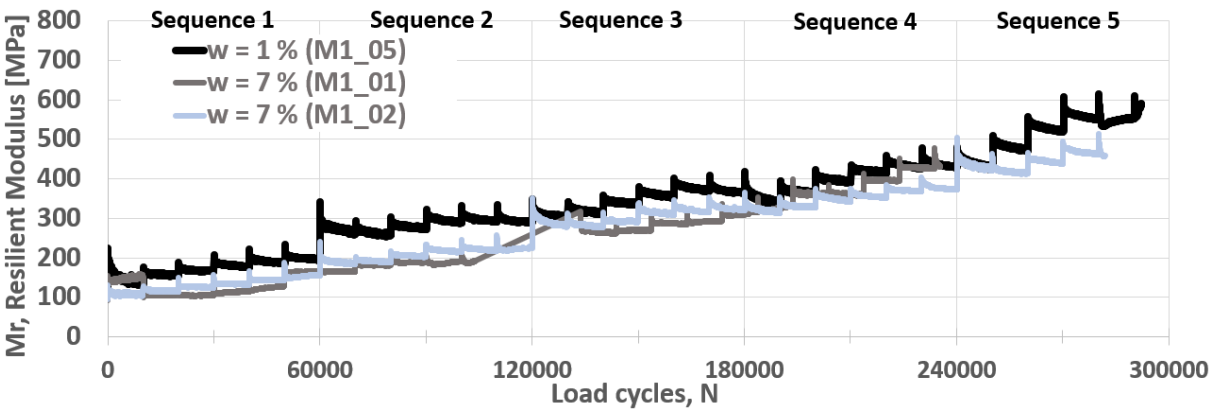

Figure 6: The observed RLTT untreated M1 quarry fines M_r, for N load cycles.

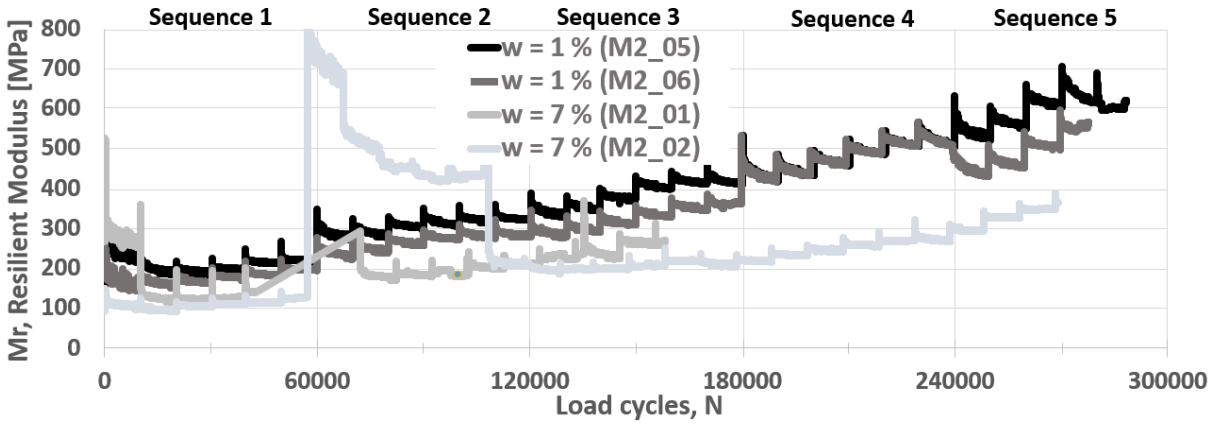

Figure 7: The observed RLTT untreated M2 quarry fines M_r, for N load cycles.

The regression fit was excellent for untreated M1 mixes. The $k-\theta$ model provided R^2 values between 0.94 and 0.97. Meanwhile, the universal model granted R^2 values from 0.96 to 0.98, demonstrating that most variability is accounted for. The universal model regression fit in a 2D $M_r - \theta$ plot (illustrating the τ_{oct}-dependency requires a 3D plot) is shown in Figure 8.

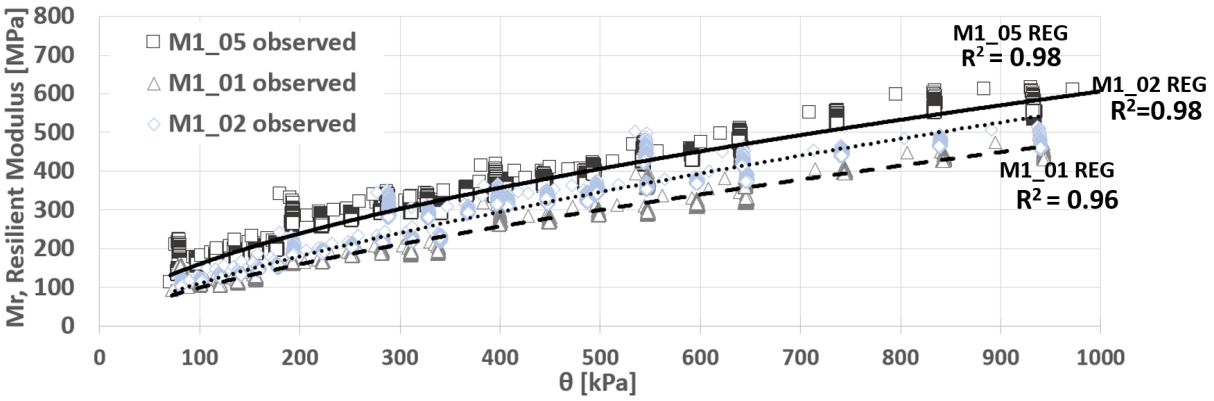

Figure 8: Universal model regression fit for untreated M1 fines in a simplified 2D $M_r - \theta$ plot.

For the untreated M2 mixes, the $k-\theta$ model R^2 was 0.92-0.93 at $w = 1$ %, but only 0.18 and 0.17 at $w = 7$ %. The poor fit at higher water content is primarily caused by anomalies in sequences 1 and 2, as could be observed from Figure 7. As with M1, the universal model performed slightly better than the $k-\theta$ model for M2, producing marginal improvements in R^2. The universal model fit for the untreated M2 material is shown in a 2D $M_r - \theta$ plot in Figure 9.

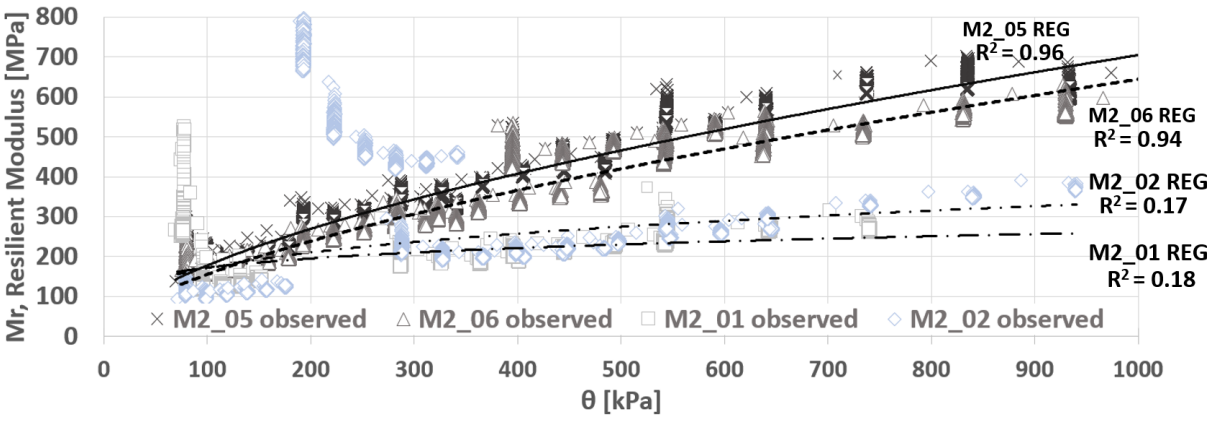

Figure 9: Universal model regression fit for untreated M2 fines, in a simplified 2D $M_r - \theta$ plot.

Resilient modulus of lignosulphonate stabilized quarry fines

The lignosulphonate stabilization procedure improves the stiffness of quarry fines; and the magnitude of stiffness increase seems substantial, but unreliable. Notably, the M_r stress-dependency is inconsistent with additives, particularly at low residual (post-cure) water content.

The additive efficacy may partially depend on the degree of curing, as shown in Figure 10. Illustratively, the M2 fines cured to a residual water content of $w_{test} = 0.4$ % was far stiffer than at $w_{test} = 1.2$ %. Also, results for the M1 samples with residual water content of 0.6 % generally fell between the 0.4 % and 1.2 % data. Nevertheless, the number of samples and parallel tests performed is insufficient to conclusively explain the apparent variation in additive effectiveness.

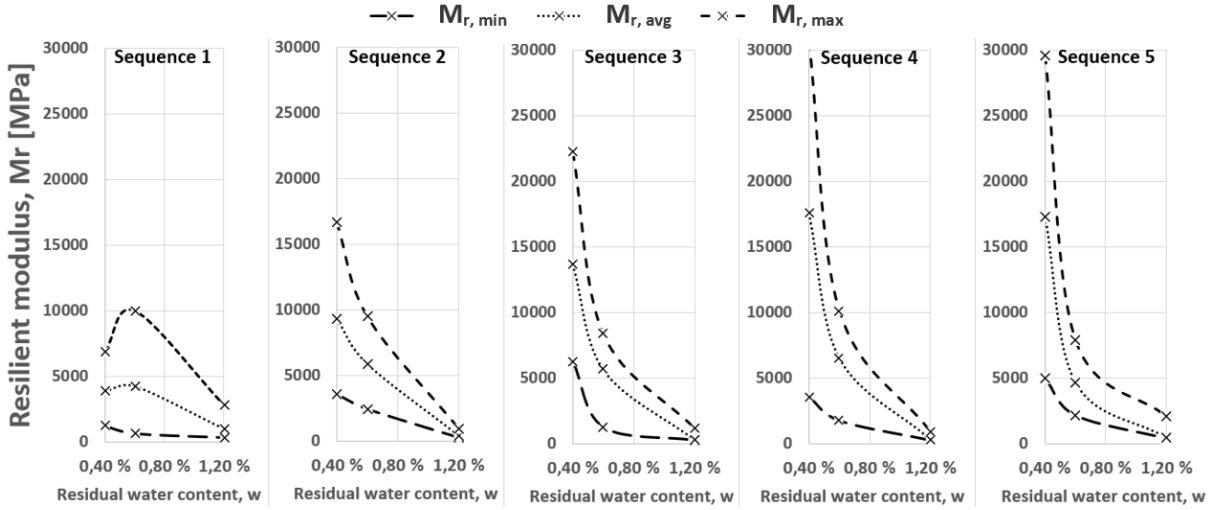

Figure 10: The observed M_r of stabilized quarry fines as a function of the residual (post-curing) water content. With separate lines for minimum ($M_{r,\ min}$), average ($M_{r,\ avg}$) and maximum ($M_{r,\ max}$) observations from each RLTT Sequence.

Due to the considerable data scatter, the M_r-model regression fit for the stabilized fines was poor. Although the universal model obtained better R^2 than the $k-\theta$ model, here the restriction on regression coefficients was detrimental to the fit quality. Thus, by removing regression sign restrictions, the universal model R^2 improved from 0.09 to 0.15, 0.41 to 0.48, 0.54 to 0.62 and 0.72 to 0.73. Curiously, the coefficient-sign deviation may imply that the material is not consistently shear-softening.

The observed M_r of the stabilized mixes, for N load cycles, is given in Figure 11. While the unrestricted universal model regression fit is provided in a 2D $M_r - \theta$ plot in Figure 12.

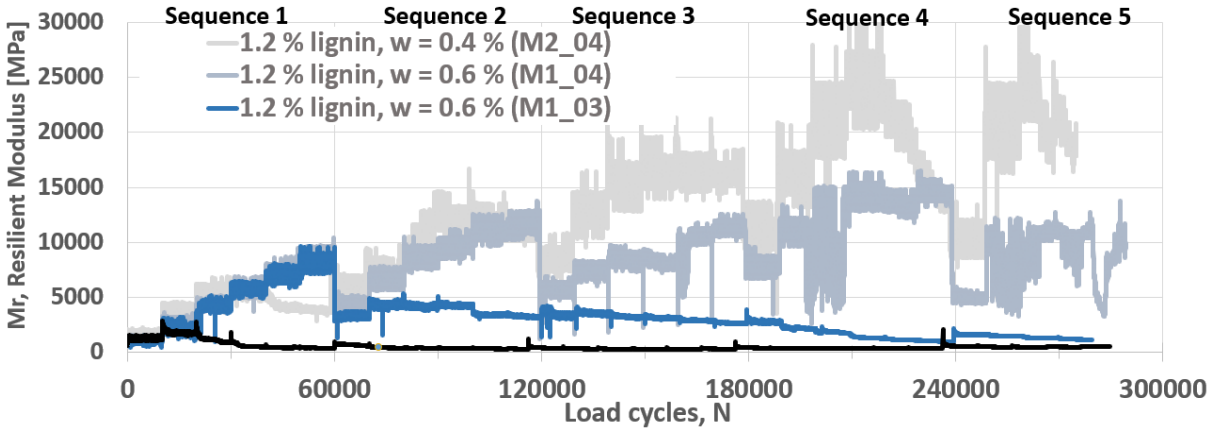

Figure 11: The observed M_r of stabilized quarry fines, for N RLTT load cycles.

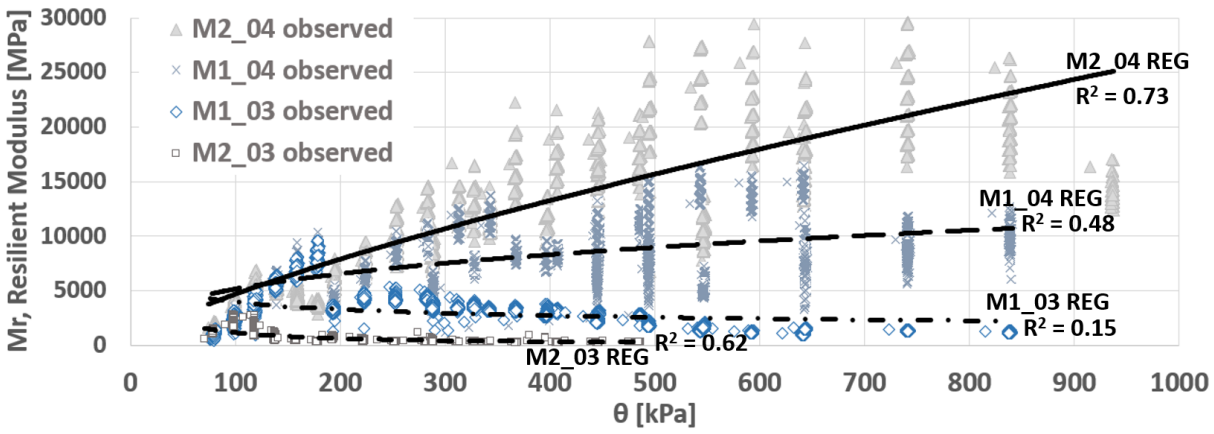

Figure 12: The universal model regression fit for stabilized fines, in a simplified 2D $M_r - \theta$ plot.

4.2 Permanent deformation assessment

Regression fits for the time-hardened Rahman, Erlingsson and Ahmed PD-model (unpublished), in equations 6-8, was determined from the RLTT results. Here, parameter b was held constant at 250, and initial value for a was equal to 1000 times $\hat{\epsilon}_p$ after stress path 1.

Similarly, as for the M_r-model regression, the PD-model regression achieved better fits for the untreated fines than for the additive treated material. Decidedly, this effect is at least partially explained by the increased stiffness post stabilization leading to very small strains; insofar as to push the LVDTs to the limit of their accuracy, which causes data-scatter. Even so, the resulting PD-model coefficients of regression achieved overall good fits, and are listed in Table 7.

Table 7: Rahman, Erlingsson and Ahmed *ERAPave* PD-model (unpublished) regression coefficients, for fixed $b = 250$.

Sample		**M1_01**	**M1_02**	**M1_03**	**M1_04**	**M1_05**	**M2_01**	**M2_02**	**M2_03**	**M2_04**	**M2_05**	**M2_06**
PD	a	0,82	0,70	2,80	0,10	0,76	1,91	0,54	0,48	0,38	0,78	0,55
model	R^2	0,98	0,98	0,99	0,63	0,97	0,99	0,99	0,98	0,74	0,99	0,95

Some of the key parameters used to evaluate PD in this research include:

- N_{max}, which is the maximum load cycles performed in the RLTT sequence (seq) before strain threshold ($\hat{\epsilon_p} = 5‰$) or manual test abortion. Therefore, a high N_{max} indicates that many or all cycles could be completed without the development of excessive PD.
- $\hat{\epsilon_p}$, which is the accumulated axial plastic strain.
- Each RLTT sequence is also categorized according to the strain rate of the last 5000 load step cycles: category A = mainly elastic, B = elasto-plastic, C = mainly plastic, "x" means the plastic strain threshold was reached (severely plastic behaviour) and "$-$" means the test was aborted (no data).

Permanent deformation properties of untreated quarry fines

As for ED properties, clearly delineating the PD properties of materials M1 and M2 is challenging from the limited available data.

Both materials M1 and M2 display a PD water susceptibility. For M1 fines, the moisture content effect on PD can be seen in Figure 13, plotting $\hat{\epsilon_p}$ as a function of applied load cycles (N), along with the PD-model regression fit. However, of note, PD of the M1 parallel samples at w = 7 % did differ markedly, making the water susceptibility difficult to quantify.

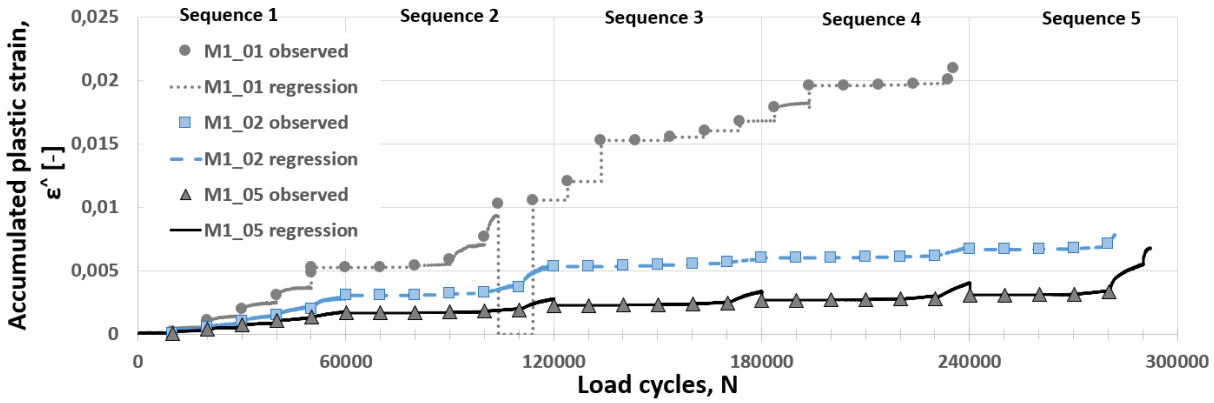

Figure 13: The RLTT accumulated axial plastic strain ($\hat{\epsilon_p}$) as a function of the applied load cycles (N) for untreated M1 fines, with *ERAPave* PD model regression.

Table 8 shows the key PD parameters from RLTTs of the untreated M1 fines. As can be seen from PD-category based on strain rate, at $w = 1$ % the first 4 load steps were largely elastic. Meanwhile, at $w = 7$ % the classifications are more unpredictable but become increasingly plastic at higher load cycles and stress.

Table 8: The RLTT PD parameters for untreated M1 fines.

seq	Untreated, $w = 7$ %														Untreated, $w = 1$ %						
	M1_01							M1_02							M1_05						
	N_{max}	$\hat{\epsilon_p}$ [‰]	ϵ' category by load step (1-6)						N_{max}	$\hat{\epsilon_p}$ [‰]	ϵ' category by load step (1-6)						N_{max}	$\hat{\epsilon_p}$ [‰]	ϵ' category by load step (1-6)					
			1	2	3	4	5	6			1	2	3	4	5	6			1	2	3	4	5	6
1	50028	5,3	B	B	C	C	C	x	60037	3,1	A	B	C	C	C	C	60041	1,7	A	B	C	B	C	C
2	54001	10,3	A	A	B	C	C	x	60032	5,3	A	A	A	B	C	C	60040	2,3	A	A	A	B	C	C
3	29708	15,3	B	C	C	x	x	x	60039	6,0	A	A	B	B	B	C	60040	2,7	A	A	A	B	C	C
4	60031	19,6	A	B	C	C	C	C	60020	6,7	A	A	B	B	B	C	60045	3,1	A	A	A	B	B	C
5	41545	20,9	A	A	B	C	-	-	42047	8,9	A	A	A	B	-	-	52096	8,1	A	A	A	C	C	x

The untreated M2 quarry fines display strong PD water susceptibility; the $w = 7$ % samples experience moderate to severe plastic deformations, while at $w = 1$ % the material behaved primarily elastic. The M2 accumulated plastic strain as a function of load cycles can be seen along with the PD-model regression in Figure 14.

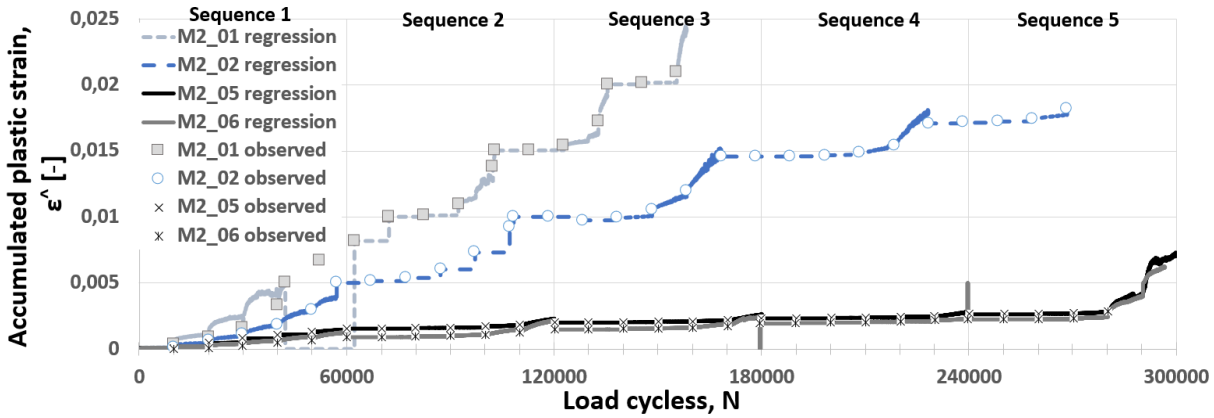

Figure 14: The accumulated axial plastic strain ($\hat{\epsilon_p}$) at N load cycles, for untreated M2 fines, with the *ERAPAve* PD-model regression. Plots for M2_05 and M2_06 are partially overlapping.

For the untreated M2 mixes, the PD reached the strain threshold fairly frequently at w = 7 %. However, at $w = 1$ %, no sequence resulted in strain threshold, and the load steps

(particularly step 1-4) could be characterized as elastic or elastoplastic. The main RLTT PD parameters for the untreated M2 fines are summarized in Table 9.

Table 9: The RLTT PD parameters for untreated M2 fines.

seq	Untreated, w = 7 %						Untreated, w = 1 %					
	M2_01			M2_02			M2_05			M2_06		
	N_{max}	$\hat{\epsilon_p}$ [‰]	ϵ' category by load step (1-6) 1|2|3|4|5|6	N_{max}	$\hat{\epsilon_p}$ [‰]	ϵ' category by load step (1-6) 1|2|3|4|5|6	N_{max}	$\hat{\epsilon_p}$ [‰]	ϵ' category by load step (1-6) 1|2|3|4|5|6	N_{max}	$\hat{\epsilon_p}$ [‰]	ϵ' category by load step (1-6) 1|2|3|4|5|6
1	42221	5,0	$B\|B\|C\|x\|x\|x$	57101	5,0	$A\|B\|C\|C\|C\|x$	60036	1,5	$A\|B\|C\|C\|C\|C$	60036	0,9	$A\|B\|C\|C\|C\|C$
2	30075	10,0	$C\|C\|C\|x\|x\|x$	51198	10,0	$A\|B\|C\|C\|C\|x$	60030	2,0	$A\|A\|A\|B\|B\|C$	60030	1,5	$A\|A\|A\|B\|C\|C$
3	30465	15,0	$A\|C\|C\|x\|x\|x$	60034	14,6	$B\|A\|C\|C\|C\|C$	60038	2,3	$A\|A\|A\|B\|B\|C$	59388	1,9	$A\|A\|A\|A\|B\|C$
4	32687	20,0	$A\|C\|C\|x\|x\|x$	60047	17,1	$A\|A\|B\|C\|C\|C$	60046	2,6	$A\|A\|A\|A\|B\|C$	60046	2,2	$A\|A\|A\|A\|B\|C$
5	22887	25,0	$A\|C\|x\|x\|x\|x$	40653	18,7	$A\|A\|B\|C\|-\|-$	60047	7,3	$A\|A\|A\|B\|C\|C$	57204	7,2	$A\|A\|A\|C\|C\|C$

Permanent deformation properties of lignosulphonate stabilized quarry fines

The RLTT results demonstrate that lignosulphonate stabilization improves the PD properties of quarry fines greatly. The additive effectiveness is evident from several observations. Firstly, post stabilization, no performed load step reached the strain threshold. Furthermore, post additive treatment, the strain rates were by and far in the elastic and the elastoplastic categories (A and B) for all load steps, as can be seen in Table 10.

Table 10: The RLTT PD parameters for lignosulphonate stabilized M1 and M2 fines.

seq	Stabilized, w = 0.6 %						Stabilized, w = 1.2 % and 0.4 %					
	M1_03			M1_04			M2_03			M2_04		
	N_{max}	$\hat{\epsilon_p}$ [‰]	ϵ' category by load step (1-6) 1|2|3|4|5|6	N_{max}	$\hat{\epsilon_p}$ [‰]	ϵ' category by load step (1-6) 1|2|3|4|5|6	N_{max}	$\hat{\epsilon_p}$ [‰]	ϵ' category by load step (1-6) 1|2|3|4|5|6	N_{max}	$\hat{\epsilon_p}$ [‰]	ϵ' category by load step (1-6) 1|2|3|4|5|6
1	60034	0,5	$B\|B\|B\|B\|B\|B$	60046	0,1	$A\|A\|A\|A\|A\|A$	60042	2,1	$A\|A\|B\|C\|C\|B$	58934	0,1	$A\|A\|A\|A\|A\|A$
2	60036	0,5	$B\|A\|A\|A\|A\|A$	59375	0,1	$A\|A\|A\|A\|A\|A$	56189	2,7	$C\|A\|C\|B\|C\|C$	60031	0,1	$B\|A\|A\|A\|A\|A$
3	59376	1,0	$A\|A\|A\|B\|B\|B$	59616	0,2	$A\|A\|A\|A\|A\|A$	60027	6,5	$B\|A\|B\|C\|C\|C$	59428	0,1	$A\|A\|A\|B\|A\|A$
4	60039	2,2	$A\|A\|B\|B\|B\|C$	59886	0,3	$A\|A\|A\|A\|A\|A$	60035	7,5	$A\|A\|A\|B\|C\|C$	60037	0,2	$A\|A\|A\|B\|B\|B$
5	40023	2,5	$A\|A\|A\|B\|-\|-$	50337	1,0	$A\|A\|A\|A\|C\|-$	48275	8,9	$A\|A\|B\|C\|C\|-$	42808	0,2	$A\|A\|A\|A\|-\|-$

From among the stabilized samples, there was 1 significant outlier: sample M2_03. With the highest residual water content, M2_03 had a markedly lower resistance to PD than the other additive treated samples. Further, M2_03 accumulated more than twice the plastic strain of the other stabilized material, by test end. The poor PD properties of M2_03 is in accordance with the ED results, which featured poor properties for the same sample as well. This difference in PD-properties is obvious from the plot of accumulated PD as a function of load cycles, along with the PD-model regression fit, in Figure 15.

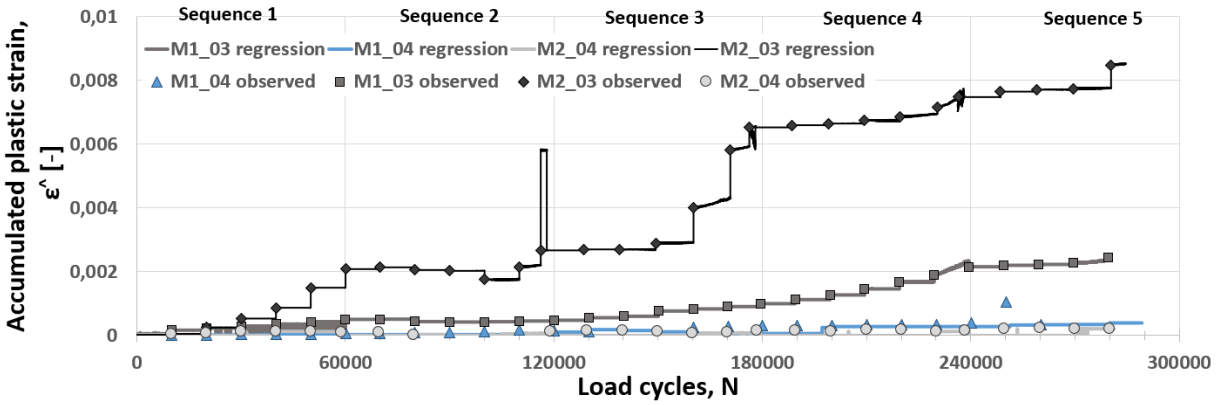

Figure 15: $\hat{\epsilon_p}$ at N load cycles for the stabilized M1 and M2 fines, with *ERAPave* PD-model regression. Curves for samples M1_04 and M2_04 are partially overlapping.

5 Numerical modeling

3 cases of quarry fines in FPLs were simulated in this research, using 2 different numerical approaches. Firstly, the FEM was used for response modeling with the software *COMSOL Multiphysics*, implementing the $k-\theta$ model. Secondly, the simpler but perhaps sufficiently accurate [50] MLLEM was used for the performance modeling with *ERAPave*, implementing the universal model. Here, the 3 primary cases of quarry fines FPLs were:

- Case 1: FPL of untreated quarry fines at high water content ($w = 7$ %).
- Case 2: FPL of untreated quarry fines at low water content ($w = 1$ %).
- Case 3: FPL of lignosulphonate stabilized quarry fines.

Due to the potentially frost susceptible nature of the untreated mixes, the stabilized case is by far the most relevant for actual engineering applications. As a compromise of material quality, stabilized fines cured to $w = 0.6$ % were selected as representative for case 3 in the simulations. While for cases 1 and 2, the overall best available fits were selected. As a result, the M_r regression coefficients used in the numerical simulations are presented in Table 11, and coefficients for performance modeling of rutting in *ERAPave* are given in Table 12.

Table 11: By case M_r-model coefficients (yielding MPa), for numerical simulation.

Case	**FPL material**	$k-\theta$ **model**			**Universal model**			
		k_1	k_2	R^2	k_1	k_2	k_3	R^2
Case 1	Unbound quarry fines ($w = 7$ %)	1.2119	0.6579	0.94	1.1702	0.8705	-0.4700	0.98
Case 2	Unbound quarry fines ($w = 1$ %)	1.9455	0.5411	0.96	1.8956	0.6991	-0.3136	0.96
Case 3	Lignosuplhonate stabilized quarry fines	47.947	0.4102	0.41	47.060	0.1288	0.6574	0.48

Table 12: By case regression coefficients (yielding unitless $\hat{\epsilon}_p$), for *ERAPave* PD-model.

Case	**FPL Material**	**Sample**	**PD model regression**		
			a	b	R^2
Case 1	Untreated quarry fines ($w = 7$ %)	M1_01	0.82	250	0.98
Case 2	Untreated quarry fines ($w = 1$ %)	M2_06	0.54	250	0.95
Case 3	Lignosulphonate stabilized quarry fines	M1_04	0.10	250	0.63

5.1 Case overview and material properties

Elastic stiffness (E or M_r), Poisson's ratio (ν) and density (ρ) of every material was needed for the simulations. The final superstructure design utilized in the analyses is listed in Table 13.

Table 13: The superstructure used for numerical simulations, with materials, thicknesses (t), resilient stiffness (E and M_r), Possion's ratio (ν) and densities (ρ).

i	**Layer**	**Material**	**Height,** t_i **[cm]**	E **or** M_r **[MPa]**	ν [-]	ρ $[kg/m^3]$	**N200**	
							$a_i \cdot t_i$	**Index =** $\Sigma(a_{i-1} \cdot t_{i-1})$
1	Wearing coarse (WC)	Asphalt, Ac11	3.5	4000	0.35	2400	10.5	0
2	Binder coarse (BC)	Asphalt, Ac11	3.0	3500	0.35	2400	9	10.5
3	Upper base layer (UBL)	Asphalt, Ag11	7.0	3000	0.35	2400	21	19.5
4	Lower base layer (LBL)	UGM, 0/32 mm	10.0	450	0.35	2100	13.5	40.5
5	Subbase layer (SBL)	UGM, 0/120 mm	70.0	300	0.35	2000	77	54
6	Frost protection layer (FPL)	Varies by case	85.0	-	0.35	2100	-	-
7	Substructure (SS)	Clay	-	15	0.35	2000	-	-

The values for the simulation material properties were selected based on recommendations from: the American *MEPDG* [29], the NPRA *Handbooks V220* [51] and *R210* [44], as well as the Swedish standards *TRVK Väg* [52] and *TRVMB 120* [53].

The simulation case superstructure is designed for 1500-8000 AADT in the opening year, exposed to 1-2 million equivalent 10 ton axles over a 20 year period. Further, the design accounted for 25 000 h^oC consecutive frost hours, for winter with a 10 year statistically expected return period. Finally, a substructure of clay was selected to ensure a conservative case with a weak and frost susceptible substructure material.

5.2 Finite element approach response modeling

Quarry fines FPLs were simulated using FEM analyses in the software *COMSOL Multiphysics*.

COMSOL Geometry

A parametric superstructure geometry was implemented for the FEM simulation. Ultimately, the selected simulation parameters were in line with Table 13. The most illustrating view of the end design is the YZ-plane, as seen in Figure 16.

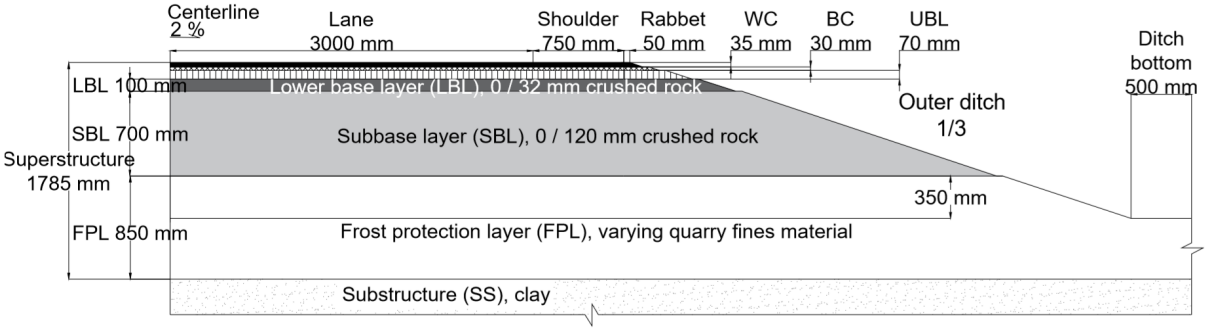

Figure 16: The superstructure geometry YZ-plane, as implemented in the *COMSOL* simulation.

The final 3D geometry and axis definition is shown in Figure 17a, with an XY-surface plane showing circular traffic loads in Figure 17b.

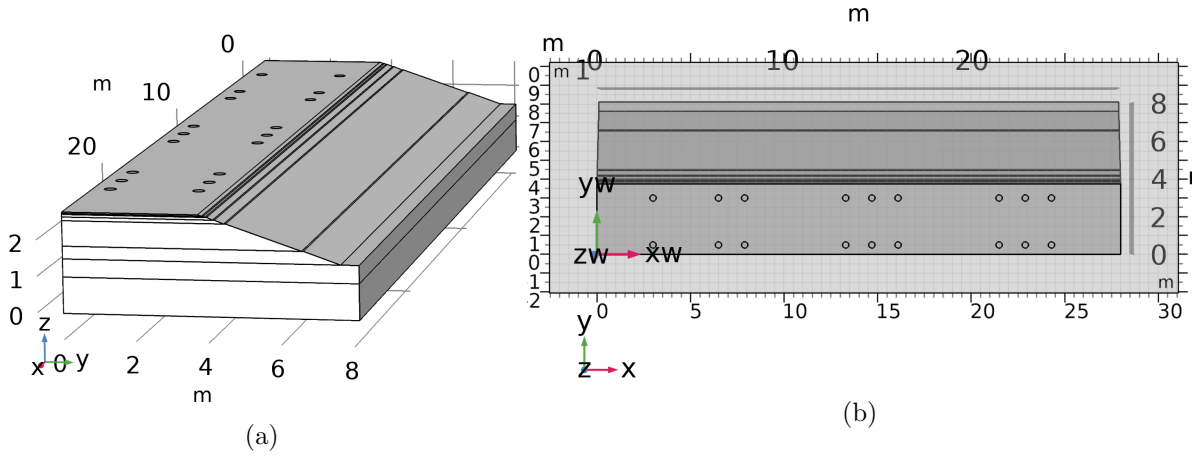

(a) (b)

Figure 17: The *COMSOL Multiphysics* 3D geometry of the simulated superstructure.

Among the central geometric and mechanical boundary conditions were the following:

- 28 meters of the profile direction (X-axis) was simulated, with a 25.25m long tandem rig, having its left side steering axle placed at $[X_0, Y_0] = [3m, 0.5m]$.

- 1 meter of the clay substructure was simulated, under which a fixed constraint was placed.
- Axial symmetry was applied on the centerline XZ-plane, with an identical lane, traffic load and ditch on the other side.

COMSOL Traffic Load

The *COMSOL* simulation accounted for gravity as well as a surface traffic load. The traffic load was a tandem rig with 4 axle groups: steering axle (single), driving axle (double), 3rd axle group (triple) and 4th axle group (triple).

All wheels were simplified as super-singles in the calculations, with the axle load uniformly distributed over a circular area with radius $r = 0.17$ m. The axle distances and the axle width were selected based on design guidelines from NPRAs *Handbook N100* [54].

The axle group loads were assigned as follows: 10 tons for steering axle, 11.5 tons for the driving axle and 16 tons each for the 3rd and 4th axle groups. This configuration may exceed the maximum allowed total weight for some roads and vehicles. A geometric layout of the vehicle load is presented in Figure 18.

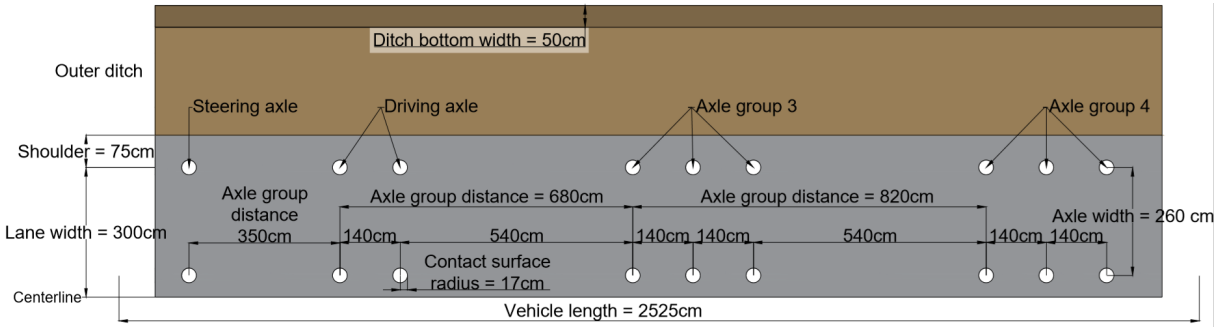

Figure 18: Overview of the traffic load for the *COMSOL* simulation, on an XY-surface plane.

COMSOL mesh and solving procedure

Solid Mechanics and *Stationary Study* was used with a *Finer* mesh, where mesh element size decreases near the load centers, as seen in Figure 19a. The M_r in the FPL was assigned the variable name *Ed* and was iterated based on a logical expression (*in*) shown in Figure 19b.

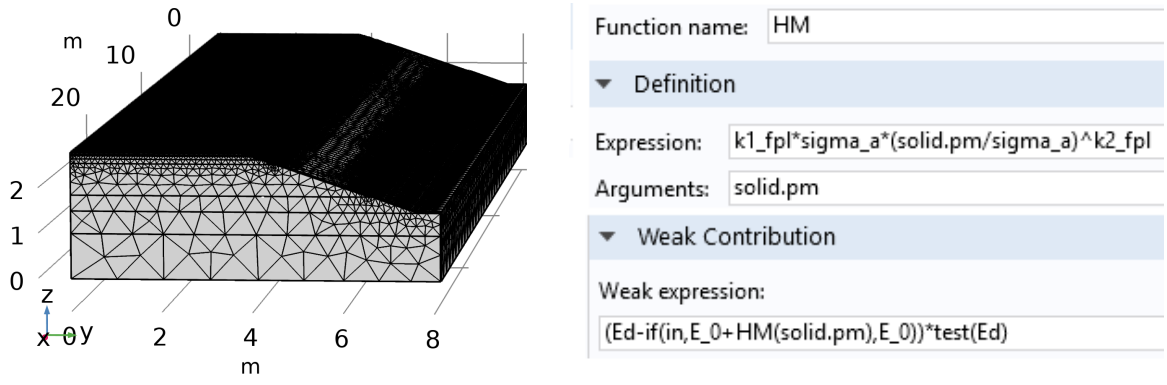

(a) (b)

Figure 19: (**a**) The COMSOL *finer* mesh and (**b**) the implementation of the non-linear elastic $k-\theta$ model (here named *HM*) for FPLs using *Weak Contribution*.

Every material layer besides the FPL was simulated using linear elasticity. For the FPL, the $k-\theta$ model was implemented using the *COMSOL* option *Weak Contribution* with an *Auxiliary*

dependent variable, and separate regression coefficients (in *COMSOL* $k_1 = k1\_fpl$ and $k_2 = k2\_fpl$) for cases 1, 2 and 3. The variation in regression coefficients was accounted for by performing a *Parametric Sweep Study* with *Specified combinations*.

The *in* boolean checks the bulk stress ($\theta = solid.pm$). For low values of θ, M_r is assigned a constant (by case) initial value $M_r = Ed = E_0$. Then, for θ increasing past set (by case) thresholds, the $k - \theta$ model (assigned function name *HM* in *COMSOL*) was utilized.

COMSOL results

Central *COMSOL* response modeling results for cases 1, 2 and 3 are presented on XY-slice planes in Figure 20, 21 and 22 respectively. Wherein, the figures display vertical stress (σ_z) near the bottom of the FPLs, and elastic vertical strain (ϵ_z) in the middle of the FPLs.

For untreated quarry fines, the bottom of the FPL experiences vertical stresses (σ_z) of approximately 35 kPa directly under the traffic load, which reduces gradually towards the outer ditch. For vertical stress, case 2 is only marginally different from case 1, meaning the water content effect on resilient modulus is not hugely influential on this parameter. However, for vertical strain, the water content effect is far more apparent; directly under the traffic load, ϵ_v was 0.05 % for case 1 and was reduced to around $\epsilon_v \approx 0.025$ % for case 2.

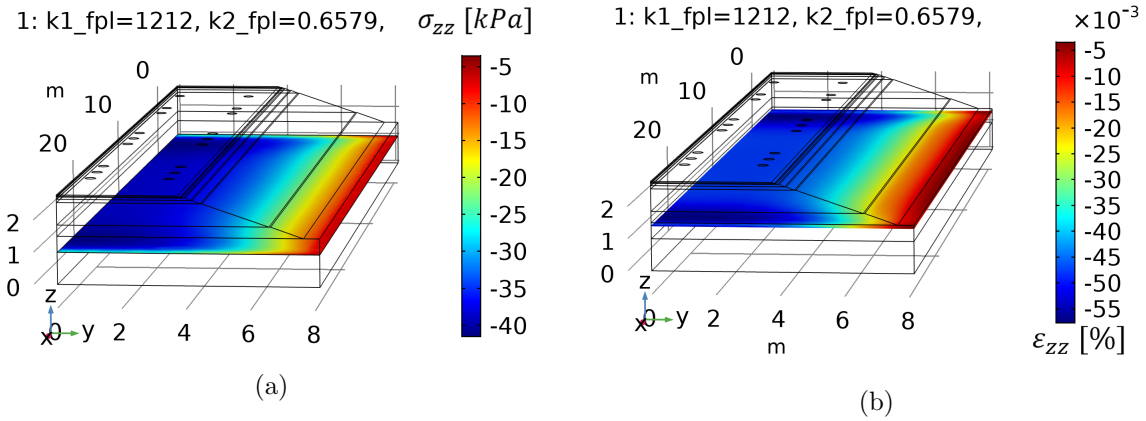

Figure 20: *COMSOL Multiphysics* case 1 results for untreated quarry fines at $w = 7$ %. (**a**) vertical stress tensor (σ_{zz} [kPa]) at the bottom of FPL ($z = 1.1m$) and (**b**) vertical strain (ϵ_{zz} [%]) levels in the middle of the FPL ($z = 1.4m$).

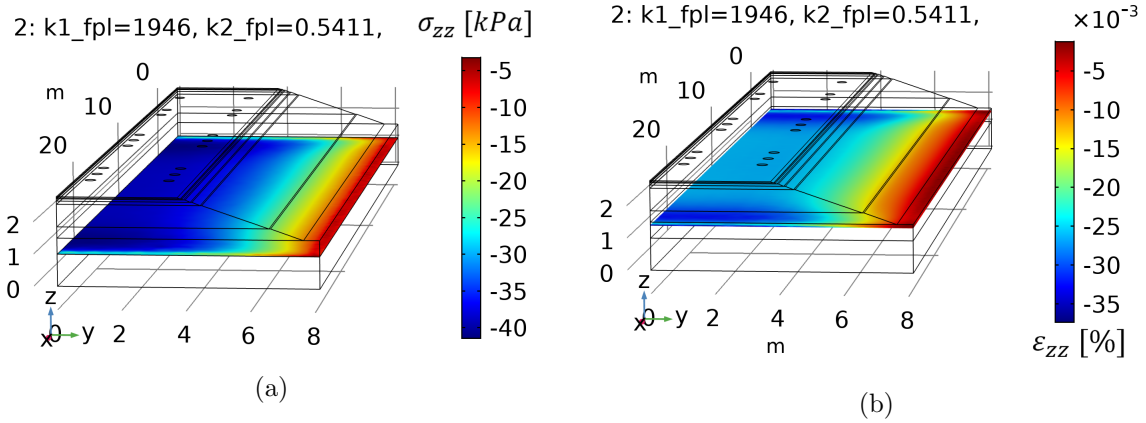

Figure 21: *COMSOL Multiphysics* case 2 results for untreated quarry fines at $w = 1$ %. (**a**) vertical stress tensor (σ_{zz} [kPa]) at the bottom of FPL ($z = 1.1m$) and (**b**) vertical strain tensor (ϵ_{zz} [%]) levels in the middle of the FPL ($z = 1.4m$).

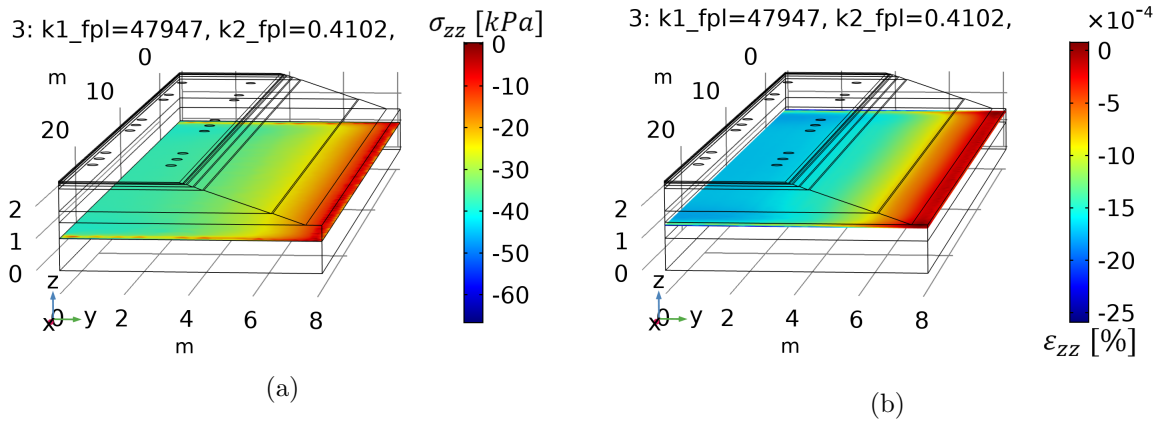

Figure 22: *COMSOL Multiphysics* case 3 results for lignosulphonate stabilized quarry fines. (**a**) vertical stress tensor (σ_{zz} [kPa]) at the bottom of FPL ($z = 1.1m$) and (**b**) vertical strain tensor (ϵ_{zz} [%]) levels in the middle of the FPL ($z = 1.4m$).

The case 3 load response results differ markedly from cases 1 and 2. Post stabilization, vertical stress at the FPL bottom is reduced by roughly 16 %, to around $\sigma_z \approx 30$ kPa. Further, with lignosulphonate additive, the vertical strains in the middle of the FPL are only $\epsilon_v \approx 0.015$ %.

In conclusion, *COMSOL* results show that vertical stress and strain levels at the depth of the quarry fines FPLs are fairly low, regardless of which case of quarry fines (stabilized or untreated) is evaluated. The traffic load is intensely distributed through the upper layers, meaning the difference in calculated stress between stabilized and untreated quarry fines FPLs is noticeable, but not staggering. Accordingly, the results indicate that the mechanical properties are sufficient for using stabilized quarry fines as road frost protection layers.

5.3 Multiple layer linear elastic approach performance modeling

The *ERAPave* load response calculations can either be done with a linear M_r, or by using the universal model [29]. For the non-linear alternative, M_r in the universal model is iterated through a relaxation factor, ω:

$$M_r^{n+1} = \omega \cdot M_r^n + (1-\omega) \cdot k_1 \cdot \sigma_a \cdot \left(\frac{\theta}{\sigma_a}\right)^{k_2} \cdot \left(\frac{\tau_{oct}}{\sigma_a} + 1\right)^{k_3} \tag{9}$$

Where: n = iteration number, $\omega = 0.5$ at default, and remaining parameters are defined in equations 2 and 3.

ERAPave climatic modeling

After implementing regional weather data from Mattmar in Sweden, a climatic elastic stiffness adjustment was performed. For UGMs, M_r was adjusted depending on in-situ water content, while an exponential temperature model was implemented for bituminous layers. The UGM climatic model stems from *MEPDG* [29]:

$$log_{10}\left(\frac{M_r}{M_{r,\ opt}}\right) = a + \frac{b-a}{1 + exp[ln(-b/a) + k_m(S - S_{opt})]} \tag{10}$$

Here, $M_{r,\ opt}$ is the resilient modulus at optimal water content for compaction. Parameters a and b are respectively minimum and maximum of $log_{10}(\frac{M_r}{M_{r,\ opt}})$, with regression parameter k_m. Meanwhile, S and S_r are degrees of saturation at a given and optimum water content (given in decimal form). Other studies were used to determine these parameters for the simulations; both

for UGMs [55], and the subgrade [29]. For the asphalt stiffness, a simple climatic exponential temperature model was used:

$$E_T = E_{T_{ref}} \cdot e^{(-b(T-T_{ref}))} \tag{11}$$

Where: E is the elastic stiffness, T is temperature and b is a material factor set to 0.065 as a simplification based on other test data [56]. The selected climatic model coefficients for both the bituminous and unbound materials used in the simulation are listed in Table 14.

Table 14: Climatic temperature (asphalt) and moisture (UGMs) model coefficients used in *ERAPave ME* response modeling, selected based on data from previous studies [29, 55, 56, 57].

Layer	**Material**	**Temperature model**	**Moisture model**		
		b	a	b	k_m
Wearing coarse (WC)	Asphalt	0.065	-	-	-
Binder coarse (BC)	Asphalt	0.065	-	-	-
Upper base layer (UBL)	Asphalt	0.065	-	-	-
Lower base layer (LBL)	UGM	-	-0.02	0.07	6.38
Subbase layer (SBL)	UGM	-	-0.01	0.20	7.20
Frost protection layer (FPL)	Varies by case	-	-	-	-
Subgrade	Clay	-	-0.59	0.40	6.13

ERAPave traffic load

The traffic load was simulated for an AADT of 5000, over a 20-year period, with 0 % traffic growth and 10 % heavy vehicles. The load equivalency factor (LEF) was set to $LEF = 1.03$. Surface stresses were calculated from single axles with single wheels, for a contact pressure of 900 kPa and axle load of 100 kN uniformly distributed over a circular area. The load-center was applied using a traffic wander with 1 standard deviation of 25 cm.

ERAPave performance modeling results

The performance modeling results show that PD within the FPL is very low for all 3 cases. Thus, the subbase layer thickness was varied to increase FPL stresses and accentuate case differences. Rut depth developed in the FPL is plotted against structural life for cases 1, 2 and 3 on Figure 23, for varying subbase layer thickness. Even at subbase thickness 0, meaning the quarry fines were functioning as both the subbase and the FPL, the rut depth was low for cases 2 and 3. This indicates that the resistance to PD is sufficient for the use of quarry fines FPLs.

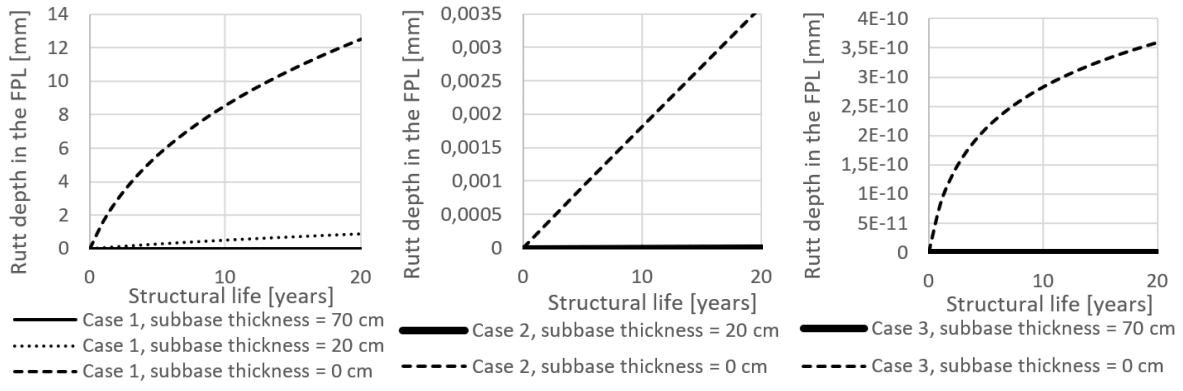

(a) (b) (c)

Figure 23: *ERAPave* performance simulation with rut depth [mm] over time for cases 1 (**a**), 2 (**b**) and 3 (**c**), using varying subbase layer thickness.

6 Conclusion

The results from both the laboratory experiments and the numerical simulations suggest that the mechanical properties of untreated and lignosulphonate stabilized quarry fines surplus are sufficient for use in FPLs. However, some of the main challenges related to the usage of quarry fines in a superstructure remain to be investigated.

Firstly, untreated quarry fines may contain significant amounts of silt, with large potential for capillary rise leading to frost heave. Also, the liquid limit of quarry fines may cause issues during the construction phase under wet conditions. Furthermore, the quarry fines may infiltrate into other layers of the structure.

Both untreated and stabilized quarry fines may be impermeable depending on additives and GSDs, causing drainage problems and pore pressure build-up affecting short term strength. Moreover, the long-term properties of stabilized quarry fines must be evaluated, accounting for effects like additive water leaching. An additional challenge could be allowing in-situ additive curing before traffic can be applied. Finally, other additives should be tested, considering availability, price and evaluating practical construction concerns for each concept.

Despite these challenges, the potential of utilizing stabilized quarry fines in FPLs seems substantial. The following main conclusions can be drawn on the mechanical properties and load response of quarry fines FPLs:

- RLTTs show that the elastic stiffness of untreated quarry fines is a non-linearly stress-dependent resilient modulus, that reduces for increasing water content. This behavior was generally well accounted for by material models based on bulk stress.
- The untreated quarry fines resilient stiffness seems fairly poor compared to most Norwegian crushed rock base- and subbase materials, but may still be sufficient for FPL use.
- Untreated quarry fines seem prone to develop excessive PD under RLTTs with low-stress levels, particularly at high water content.
- Lignosulphonate stabilization of quarry fines increases resilient modulus, but from the available sample size, the increase is not predictable and may depend on residual water content post-cure.
- The resistance to PD in quarry fines material is improved by a large margin through lignosulphonate additive. Stabilized quarry fines do not develop excessive PD under RLTTs with low-stress levels, and RLTT load step strain rates are mainly elastic and elastoplastic for stabilized quarry fines mixes.
- For lignosulphonate stabilized quarry fines, the $k - \theta$ and universal resilient modulus models perform poorly, partially explained by less stress-dependent resilient properties than conventional UGMs. At high stiffness, the strains are also small, decreasing LVDT accuracy and causing data scatter.
- FEM and MLLEM simulation results imply that the mechanical properties of stabilized quarry fines are sufficient for use in FPLs exposed to medium traffic.

7 Acknowledgements

This master's thesis was financed with scholarships from Asplan Viak and the Norwegian Public Roads Administration. The quarry fines materials were provided from the quarry free of charge. NTNU postdoc Diego Barbieri aided in data analyses and performing experiments and should be credited along with main project guide professor Inge Hoff if this work is published.

References

[1] H. Holen. NFF Report Series - Report 11: TBM Tunnelling, Chapter 13: TBM vs Drill Blast Tunneling. Technical report, The Norwegian Tunnelling Society (NFF), 2014. `http://nff.no/wp-content/uploads/2014/01/Publication_11.pdf`.

[2] NPRA. *Håndbok N200 Vegbygging*. The Norwegian Public Roads Administration (NPRA) and Road Directorate, 2019. [In Norwegian].

[3] Bane NOR. *Teknisk regelverk*. Bane NOR SF, 2020. `https://trv.banenor.no/wiki/Forside` [In Norwegian].

[4] Standard Norge. *Aggregates for railway ballast, NS-EN 13450:2002+NA:2009*. Standard Norge, (2016-12-01) edition, 2016. ICS 91.100.15 and 91.100.30 [In Norwegian].

[5] Standard Norge. *Aggregates for concrete, NS-EN 12620:2002+A1:2008+NA:2016*. Standard Norge, (2009-01-01) edition, 2009. ICS 93.100 [In Norwegian].

[6] NGU. *The Aggregate Material Deposit Database (grus- og pukkdatabasen)*. The Norwegian Geolocial Survey (NGU), 2020. `http://geo.ngu.no/kart/grus_pukk/` [In Norwegian].

[7] R. Dahl, K. Wolden, E. Erichsen, A. Ulvik, P.-R. Neeb, and K. Riiber. Sustainable management of aggregate resources in Norway. *Bulletin of Engineering Geology and the Environment*, 71(2):251–255, 2012.

[8] DIRMIN. Harde fakta om mineralnæringen, mineralstatistikk 2019. Technical report, The Directorate of Mining with the Commissioner of Mines at Svalbard, 2018. [In Norwegian].

[9] NFF. Tunnelling statistics. Norwegian Tunnelling Society (NFF), 2019. `http://nff.no/nyheter-og-tall/fagstoff/tunnelstatestikk/` [In Norwegian].

[10] K. Aarstad, B. G. Petersen, C. R. Martinez, D. Gunther, J. Macias, L. U. Mathisen, M. Fladvad, R. Haugen, M. K.and Nålsund, S. W. Danielsen, and Ø. Bjøntegaard. Local use of rock materials – production and utilization State-of-the-art. Technical report, SINTEF, 2019.

[11] A. Dino, G, S. W. Danielsen, C. Chiappino, and C. J. Engelsen. Recycling of rock materials as part of sustainable aggregate production in Norway and Italy. *Quarterly Journal of Engineering Geology and Hydrogeology*, 50(4):412–416, 2017.

[12] S. W. Danielsen and E. Kuznetsova. Resource management and a best available concept for aggregate sustainability. *Geological Society of London Special Publications*, 416(1):59–70, 2016.

[13] NGU. The Norwegian Geolocial Survey (NGU) quarternary period Norwegian soil map (kvartærgeologisk kart). Public database, 2020. `http://geo.ngu.no/kart/losmasse/` [In Norwegian].

[14] Standard Norge. *NS-EN ISO 14688-1:2018, Geotekniske felt- og laboratorieundersøkelser - Identifisering og klassifisering av jord - Del 1: Identifisering og beskrivelse*. Standard Norge, (2018-05-01) edition, 2018.

[15] M. Fladvad. Utilization of unbound aggregates for road construction. *Norsk Bergforening, Mineralproduksjon*, 2017.

[16] M. Fladvad, J. Aurstad, and B. J. Wigum. Comparison of practice for aggregate use in road construction — results from an international survey. In *The 10th International Conference on the Bearing Capacity of Roads, Railways and Airfields (BCRRA 2017)*. CRC Press, 2017. DOI 10.1201/9781315100333-81.

[17] NPRA. *Håndbook R762 Prosesskode 2*. The Norwegian Public Roads Administration (NPRA) and Road Directorate, 2018. [In Norwegian].

[18] Y. Zhang, L. K. Korkiala-Tanttu, H. Gustavsson, and A. Miksic. Assessment for Sustainable Use of Quarry Fines as Pavement Construction Materials: Part I - Description of Basic Quarry Fine Properties. *Materials*, 12(8), 2019.

[19] Y. Zhang, L. K. Korkiala-Tanttu, and M. Borén. Assessment for Sustainable Use of Quarry Fines as Pavement Construction Materials: Part II - Stabilization and Characterization of Quarry Fine Materials. *Materials*, 12(15), 2019.

[20] B. J. Wigum, S. W. Danielsen, O. Hotvedt, and B. Pedersen. Production and utilisation of manufactured sand: State-of-the-art report. Technical report, SINTEF Building and Infrastructure, Oslo, 2009.

[21] R. G. Hicks and C. L. Monismith. Factors influencing the resilient properties of granular materials. *Highway Research Record*, 345:15–31, 1971.

[22] F. Lekarp, U. Isacsson, and A. Dawson. State of the Art. II: Permanent Strain Response of Unbound Aggregates. *Journal of Transportation Engineering*, 126(1):76–83, 2000.

[23] H. H. Titi, H. Tabatabai, and A. Faheem. Evaluation of the Long-Term Degradation and Strength Characteristics of In-situ Wisconsin Virgin Base Aggregates under HMA Pavements. Final report, WHRP 0092-15-06, Department of Civil Engineering and Mechanics, University of Wisconsin-Milwaukee, Champaign, Illinois, 2018.

[24] G. Canon Falla, S. Leischner, A. Blasl, and S. Erlingsson. Characterization of unbound granular materials within a mechanistic design framework for low volume roads. *Transportation Geotechnics*, 13:2–12, 2017.

[25] F. Lekarp, U. Isacsson, and A. Dawson. State of the Art. I: Resilient Response of Unbound Aggregates. *Journal of Transportation Engineering*, 126(1):66–75, 2000.

[26] J. Uzan. Characterisation of granular material. *Transportation Research Record*, N1022:52–59, 1985.

[27] T. C. Hopkins, T. L. Beckham, and C. Sun. Resilient modulus of compacted crushed stone aggregate bases. Research report, KTC-05-27/SPR-229-01-1F, Kentucky Transportation center, University of Kentucky in cooperation with Kentucky DOT and the Federal Highway Association, Kentucky, 2007.

[28] NCHRP. 1-28A Harmonized test methods for laboatory determination of resilient modulus for flexible pavement design. Final report, National Cooperative Highway Research Program, Transport Research Board, Tempe, Arizona, 2003.

[29] NCHRP. 1-37A Guide for Mechanistic-Empirical Design of new and rehabilitated pavement structures. Final report, National Cooperative Highway Research Program, Transport Research Board, Champaign, Illinois, 2004.

[30] M. W. Witzak and J. Uzan. *The universal airport pavement design system. Report 1 of 4, Granular Material Characterization*. University of Maryland, College Park, 1988.

[31] M. Souliman, M. Mamlouk, C. Zapata, and C. Cary. Data Collection to Support Implementation of the Mechanistic-Empirical Pavement Design Guide for County Roads. *Transportation Research Record*, Vol.1(2225):67–77, 2011.

[32] Z. Hossain, M. Zaman, and C.; Doiron. Mechanistic Empirical Pavement Design Guide Input Parameters for Unbound Aggregates in Oklahoma. *IACGE 2013: Challenges and Recent Advances in Geotechnical and Seismic Research and Practices*, Series: GSP 232:578–585, 2013.

[33] S. Werkmeister, A. Dawson, and F. Wellner. Permanent deformation behavior of granular materials and the shakedown concept. *Transportation Research Record*, 1757:75–81, 2001.

[34] S. Werkmeister. *Permanent deformation behavior of unbound granular materials.* PhD thesis, University of technology, Dresden, Germany, 2003.

[35] L. Uthus. *Deformation Properties of Unbound Granular Aggregates.* PhD thesis, The Norwegian University of Science and Technology (NTNU), Trondheim, 2007.

[36] I. Hoff, L. Bakløkk, and J. Aurstad. Influence of laboratory compaction method on unbound granular materials. In *Proceedings for the 6th International Symposium on Pavements Unbound (UAR 6)*, 2003.

[37] I. Hoff. *Material properties of unbound aggregates for pavement structures.* PhD thesis, The Norwegian University of Science and Technology (NTNU), Trondheim, 1999.

[38] S. Erlingsson. Modelling of rutting development in pavement structures. *Transport Research Arena 2012*, 48:321–330, 2012.

[39] M. S. Rahman and S. Erlingsson. Predicting permanent deformation behaviour of unbound granular materials. *International Journal of Pavement Engineering*, 16(7):1–15, 2015.

[40] K.-H. Tseng and R. L. Lytton. Prediction of permanent deformation in flexible pavement materials. *Implication of aggregates in the design, construction, and performance of flexible pavements*, pages 154–72, 1989.

[41] L. Korkiala-Tanttu. A new material model for permanent deformations in pavements. In *Proceedings of the international conferences on the bearing capacity of roads, railways and airfields*, 05 2005.

[42] M. S. Rahman and S. Erlingsson. A model for predicting permanent deformation of unbound granular materials. *Road Materials and Pavement Design*, 16(3):1–21, 2015.

[43] S. Erlingsson and M. S. Rahman. Evaluation of permanent deformation characteristics of unbound granular materials by means of multistage repeated-load triaxial tests. *Journal of the transportation research board*, 2069:11–19, 2013.

[44] NPRA. *Håndbok R210 Laboratorieundersøkelser.* Statens Vegvesen and Vegdirektoratet, 2016. [In Norwegian].

[45] ASTM. *Standard Test Method for Methylene Blue Index of Clay, ASTM C837.* ASTM international, 2019.

[46] R. Nålsund. *Railway Ballast Characteristics, Selection Criteria and Performance.* PhD thesis, The Norwegian University of Science and Technology (NTNU), Trondheim, 2014.

[47] D. Barbieri. *Use of local material in road construction.* PhD thesis, The Norwegian University of Science and Technology (NTNU), Trondheim, 2019.

[48] Standard Norge. *Mekanisk stabiliserte og hydraulisk stabiliserte masser - Del 7: Syklisk treaksialprøving for mekanisk stabiliserte masser*. Standard Norge, 1 (2004-03-10) edition, 2004. ICS 93.080.20 [In Norwegian].

[49] Borregaard. Dustex HSE product declaration, 2020. `https://www.dustex.no/content/download/107272/19499057/file/Dustex__Sikkerhetsdatablad.pdf` [In Norwegian].

[50] T. Saevarsdottir and S. Erlingsson. Road materials and pavement design modelling of responses and rutting profile of a flexible pavement structure in a heavy vehicle simulator test. *Road Materials and Pavement Design*, 16(1), 2014.

[51] NPRA. *Håndbok V220 Geoteknikk i vegbygging*. Statens Vegvesen and Vegdirektoratet, 2018. [In Norwegian].

[52] Trafikverket. *TRVK Väg, Trafikverkets tekniska krav Vägkonstruktion*. Trafikverket, 2011. ISBN: 978-91-7467-137-7`https://trafikverket.ineko.se/Files/sv-SE/10750/RelatedFiles/2011_072_TRVK_vag_2.pdf` [In Swedish].

[53] Vägverket. *VVMB 120 Inventering och värdering av befintlig väg*. Vägverket, 2009. ISSN: 1401-9612 `https://trafikverket.ineko.se/Files/sv-SE/11007/RelatedFiles/2009_106_vvmb_120_inventering_och_vardering_av_befintlig_vag.pdf` [In Swedish].

[54] NPRA. *Håndbok N100 Veg- og gateutforming*. The Norwegian Public Roads Administration (NPRA) and Road Directorate, 2018. [In Norwegian].

[55] Mohammad Shafiqur Rahman and Sigurdur Erlingsson. Moisture influence on the resilient deformation behaviour of unbound granular materials. *International Journal of Pavement Engineering*, Vol.17(9):763–775, 2015.

[56] S. Erlingsson. Modelling of Rutting Development in Pavement Structures. *Procedia - Social and Behavioral Sciences*, 48(C):321–330, 2012.

[57] F. Salour and S. Erlingsson. Resilient modulus modelling of unsaturated subgrade soils: laboratory investigation of silty sand subgrade. *Road Materials and Pavement Design*, 16(3):553–568, 2015.

A Appendix

A.1 Consequences of the Covid-19 pandemic

NTNU
Faculty of Engineering
Department of Civil and Environmental Engineering

Date
3 June 2020
Your date

Our reference

Your ref

To Whom it Might Concern

Master thesis spring 2020 - consequences of the Covid 19 pandemic

The pandemic situation in spring 2020 made it necessary to change or adjust the topic for master theses at NTNU. The university closed including laboratories and did not allow any type of field work, thus made it impossible to continue planned work for many students.

Sincerely yours

Inge Hoff
Professor

This letter was sent to all students with specialisation in Transport, Road or Railways in the Civil and Environmental study program to be included as an attachment in their thesis.

Address
7491 Trondheim
Norway

Org. no. 974 767 880
postmottak@iv.ntnu.no
www.ntnu.no/ibm

Location
Høgskoleringen 7 A

Phone
+47 73594640

Executive officer
Inge Hoff
inge.hoff@ntnu
Phone: 934 26 463

Please address all correspondence to the organizational unit and include your reference.

A.2 Norwegian Abstract / Norsk sammendrag

Formålet med dette studiet er å vurdere de mekaniske egenskapene til tilslags-finstoff, for å evaluere potensialet av å benytte materialet i frostsikringslag i veier. Tilslags-finstoff er underutnyttede overskuddsmaterialer, noe som medfører at nye anvendelser burde utvikles. Derfor ble resilient modulen til to 0/4 mm tilslagsmaterialer bestemt ved hjelp av sykliske treaksialforsøk. Deretter ble lastresponsen til ubundne og lignosulfonat stabiliserte tilslags-finstoff simulert ved numerisk modellering.

12 sykliske treaksialforsøk ble utført med multistage procedure ved lave spenningsnivå. Tilslags-finstoffet ble testet ubundet med 1 % og 7 % vanninnhold, samt med 1.2 % herdet lignosulfonat, for å vurdere effekten av stabilisering med bindemiddel. Resilient modulen i det ubundne materialet var omkring 100-300 MPa for sekvens 1 spenningsnivåer: σ_d på 20-120 kPa og $\sigma_t = 20$ kPa. Stabilisering med tilsetningsstoffer økte stivheten med en stor, men inkonsekvent margin; ettersom stabilisert resilient modul lå på 400-10000 MPa for de samme sekvens 1 spenningene.

En optimalisert tilpasning til $k - \theta$- og den universelle ocrahedral resilient modul modellen ble etablert ved hjelp av regresjonsanalyse. Den universelle modellen oppnådde R^2 >0.90 for de fleste ubundne prøvene. Derimot var spredningen i data betydelig etter bindemiddel stabilisering, noe som resulterte i $R^2\epsilon$[0.15,0.73].

Lignosulfonat tilsetningen forbedret også mostand mot permanente deformasjoner i tilslags-finstoffet enormt. Spesifikt, ble observert akkumulert plastisk tøyning i treaksialtestene cirka halvert gjennom herdeprosessen. Videre viste treaksiale laststeg langt mer elastisk enn plastisk oppførsel etter stabilisering. Fra disse resultatene ble så en beste tilpasning til en tids-herdet permanent deformasjons-modell utført.

Stabiliserte og ubundne tilslags-finstoff i frostsikringslag ble simulert ved flerlags lineære elastiske og elementmetode analyser, via henholdsvis ERAPave og COMSOL Multiphysics. Simuleringene tok hensyn til ikke-lineær materialoppførsel ved hjelp av de spenningsavhengige regresjonsmodellene som ble opparbeidet fra eksperimentene.

Under lasten av et modulvogntog indikerer den beregnede lastresponsen i tilslags-finstoffs frostsikringslagene at de mekaniske egenskapene er tilstrekkelige for bruk av konseptet. Resultat fra simulering av permanent deformasjon støtter denne konklusjonen, og tyder på at materialet ikke vil utvikle uakseptable permanente deformasjoner ved en eksponering av middels trafikk.

A.3 List of figures

List of Figures

A.4 List of tables

List of Tables

B Appendix - Supplementary RLTT data

B.1 M1_01 supplementary RLTT data

Sample	M1_01
Water content, *w*	7 %
Additive	-

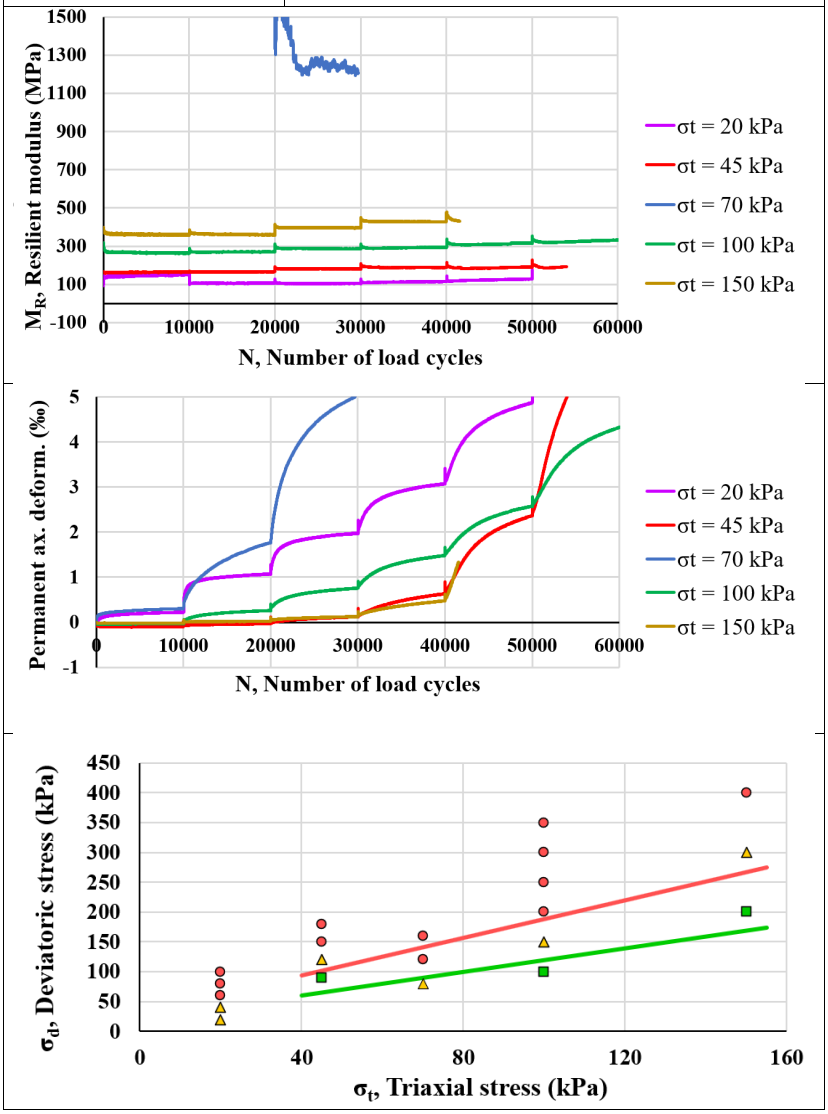

B.2 M1_02 supplementary RLTT data

Sample	M1_02
Water content, *w*	7 %
Additive	-

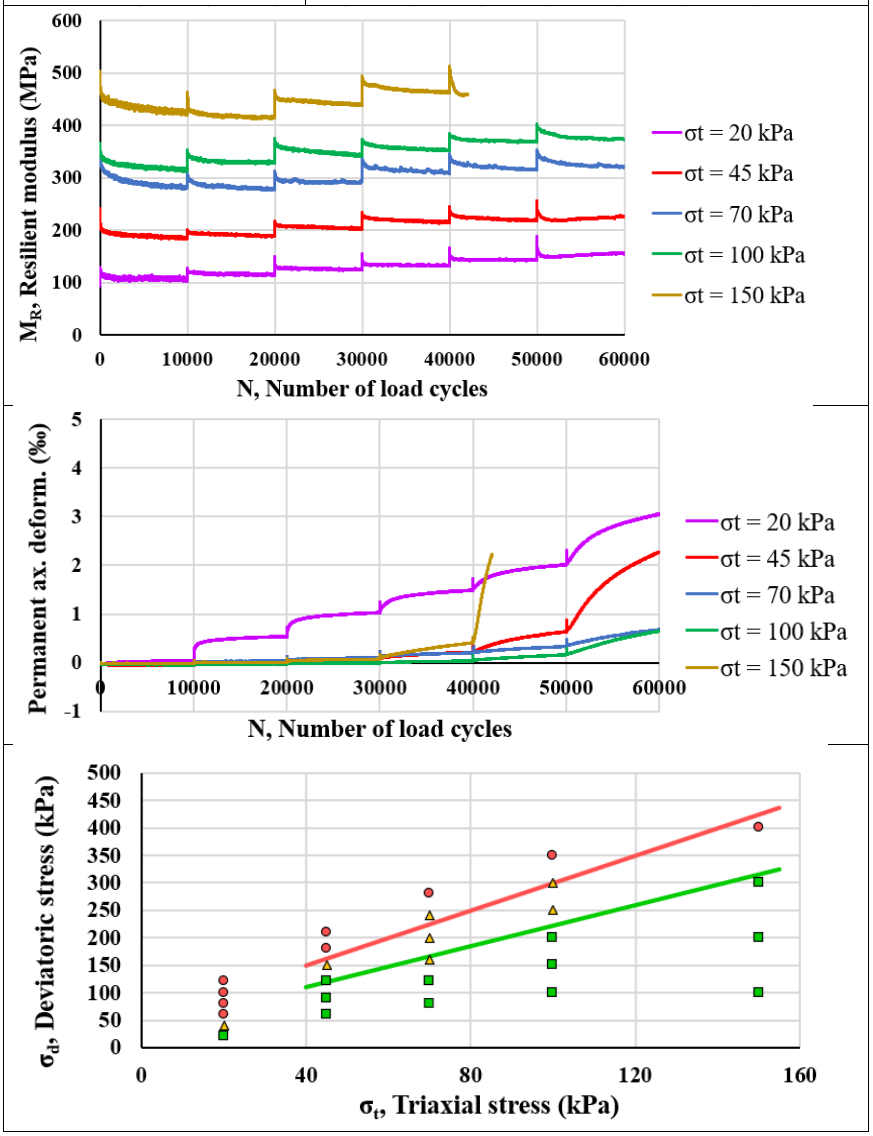

B.3 M1_03 supplementary RLTT data

Sample	M1_03
Water content, *w*	0.6 % at test
Additive	1.2 % lignin

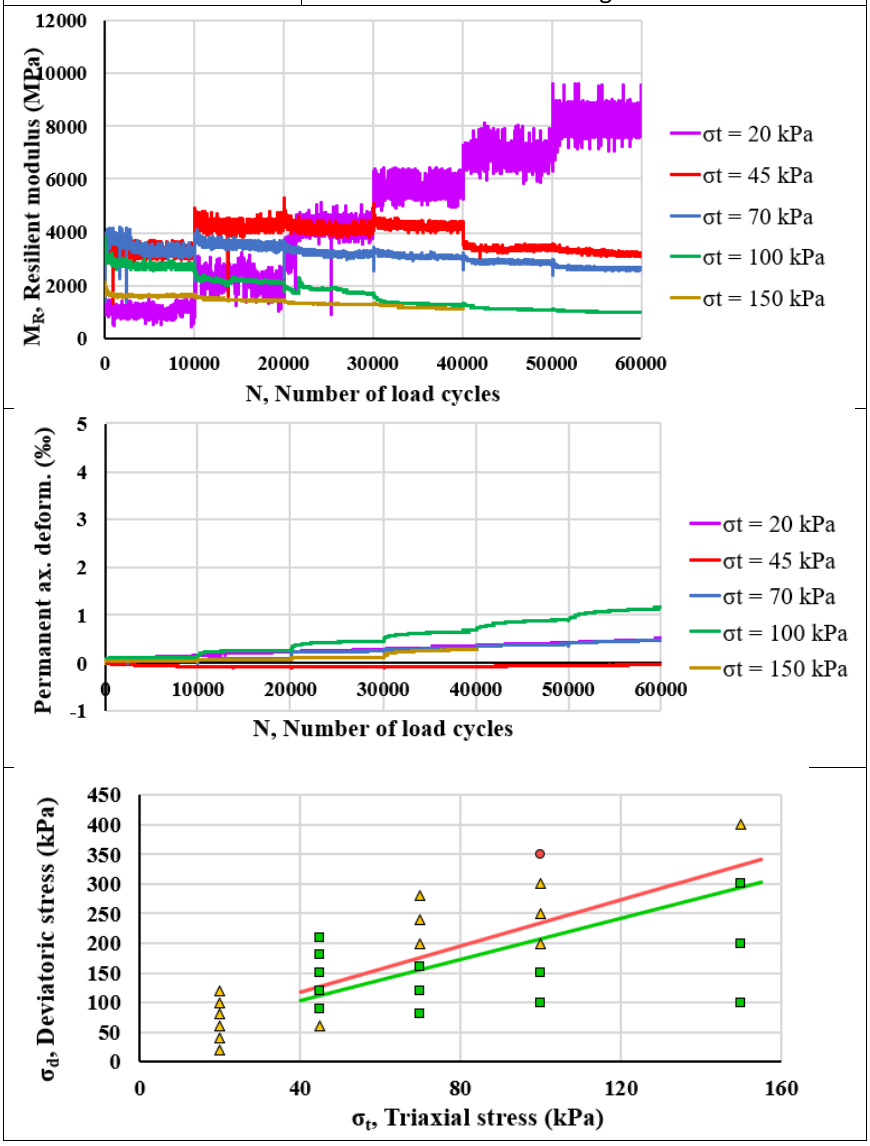

B.4 M1_04 supplementary RLTT data

Sample	M1_04
Water content, *w*	0.6 % at test
Additive	1.2 % lignin

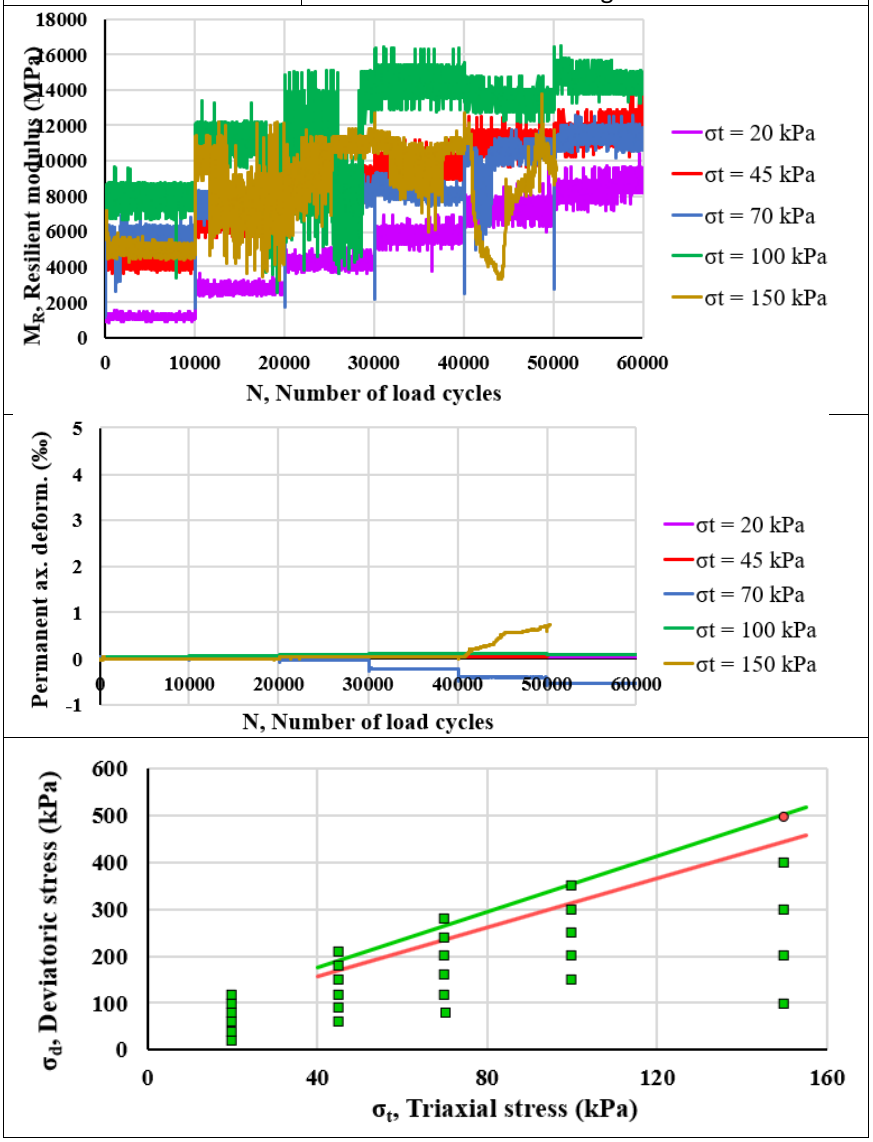

B.5 M1_05 supplementary RLTT data

Sample	M1_05
Water content, *w*	1 %
Additive	-

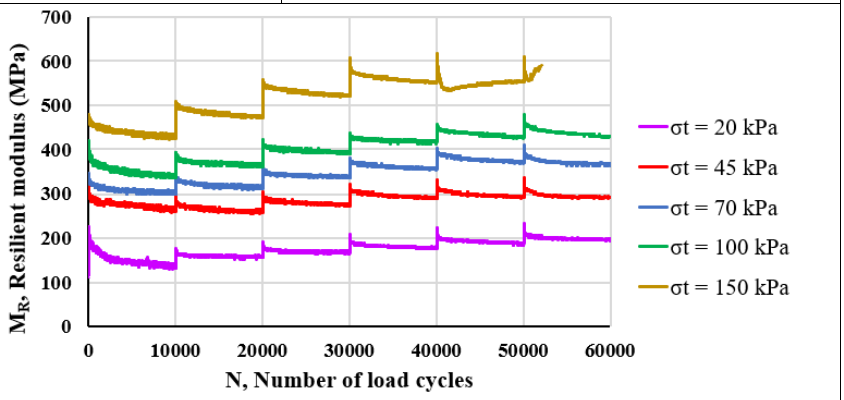

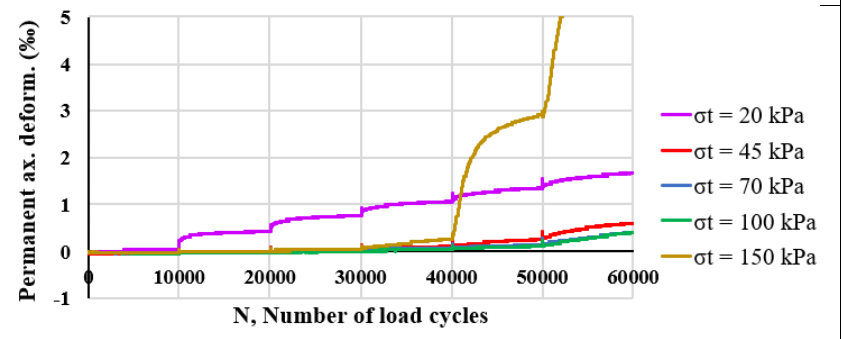

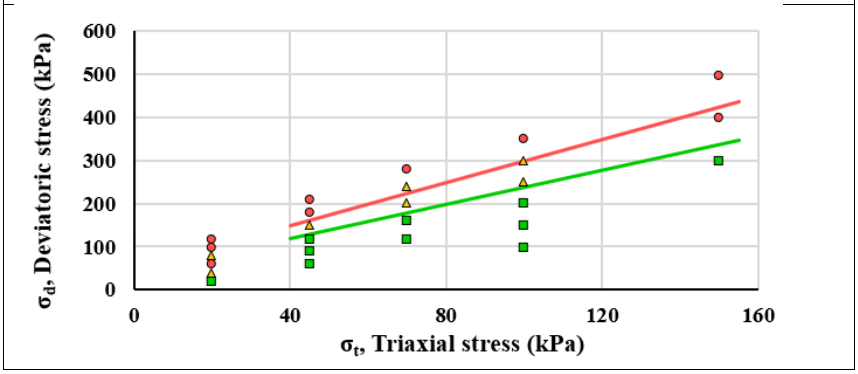

B.6 M2_01 supplementary RLTT data

Sample	M2_01
Water content, *w*	7 %
Additive	-

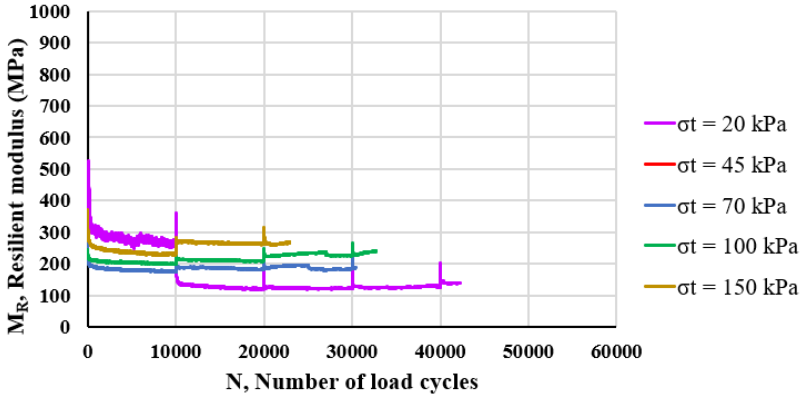

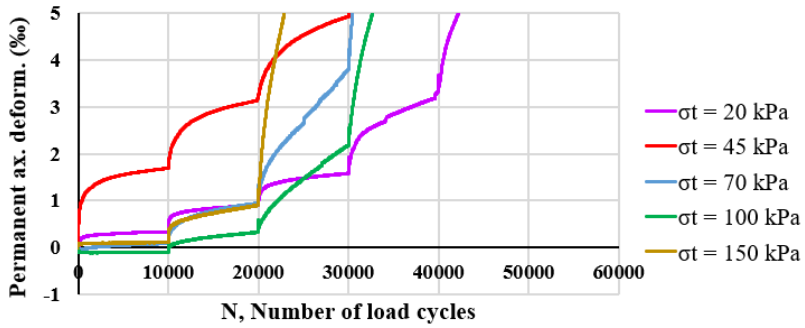

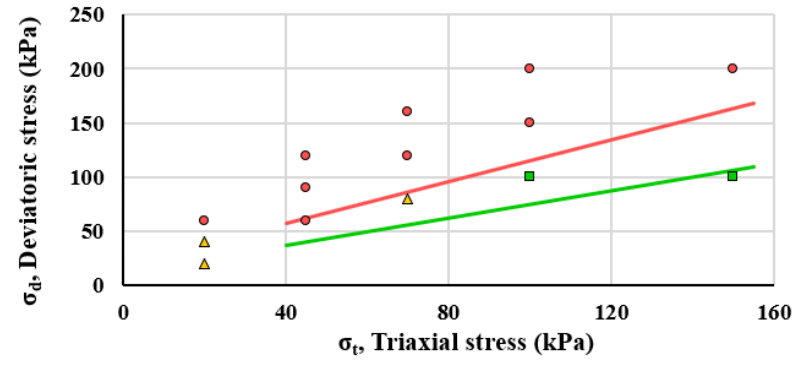

B.7 M2_02 supplementary RLTT data

Sample	M2_02
Water content, *w*	7 %
Additive	-

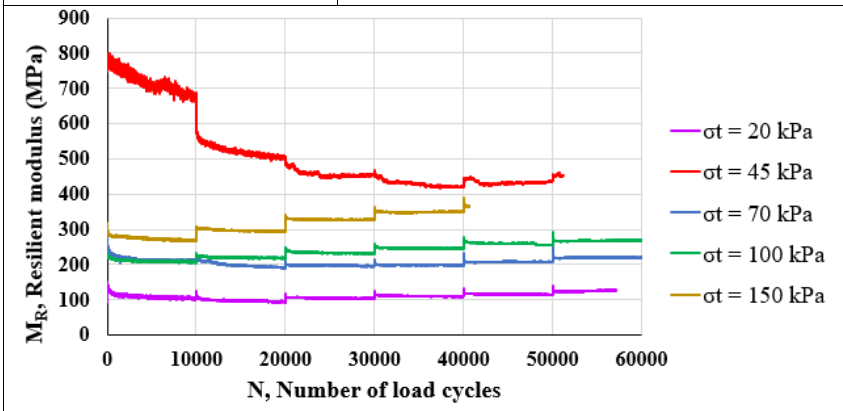

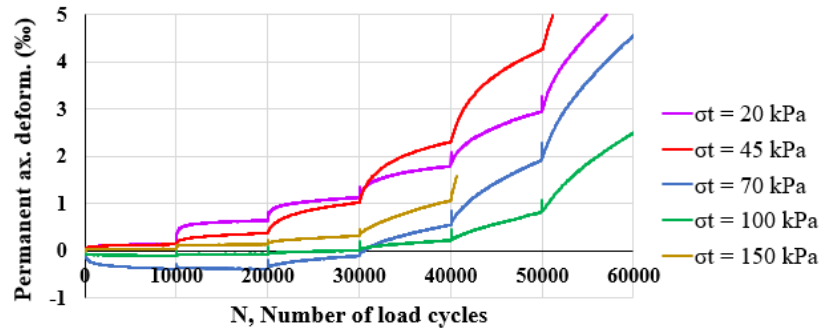

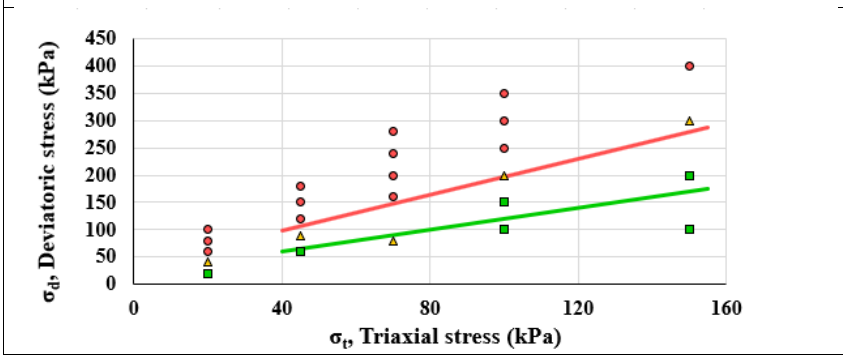

B.8 M2_03 supplementary RLTT data

Sample	M2_03
Water content, *w*	1.2 % at test
Additive	1.2 % lignin

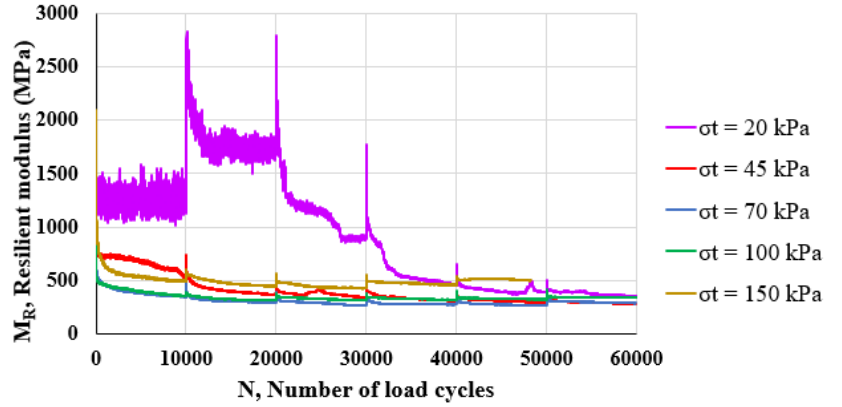

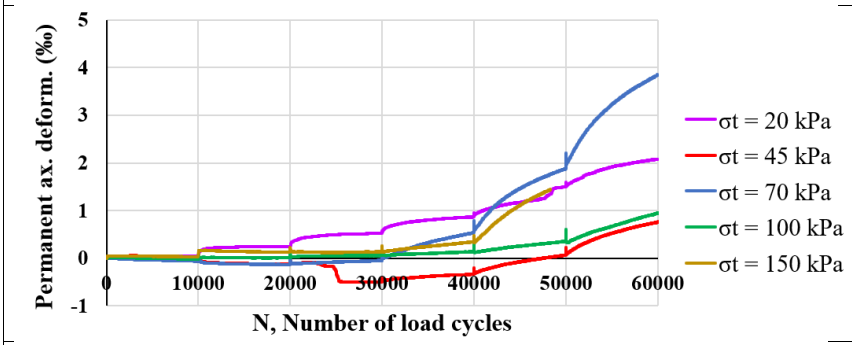

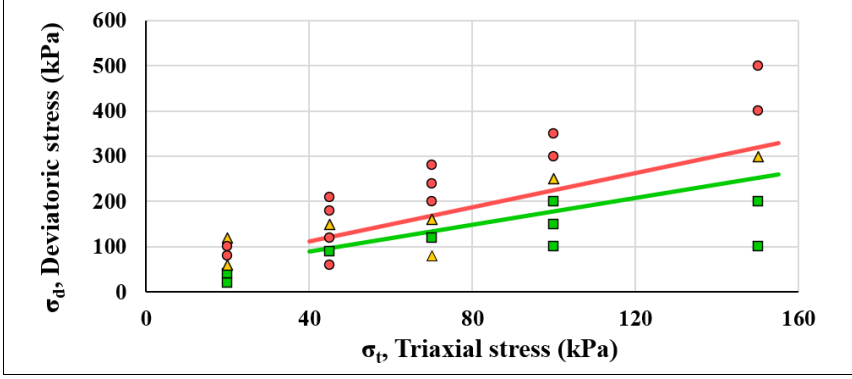

B.9 M2_04 supplementary RLTT data

Sample	M2_04
Water content, *w*	0.4 % at test
Additive	1.2 % lignin

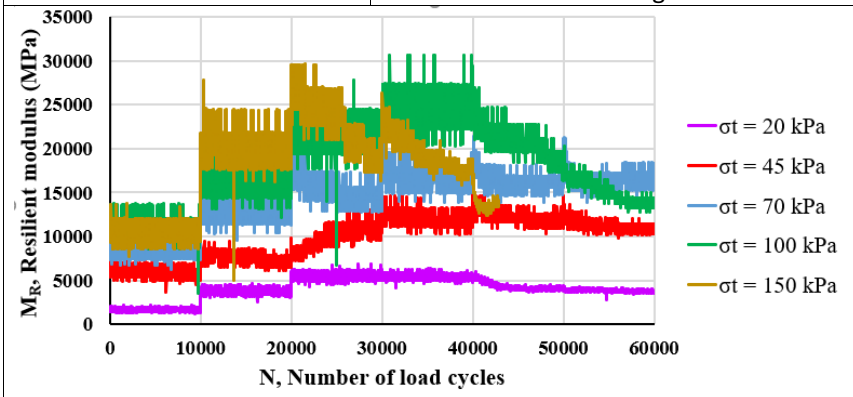

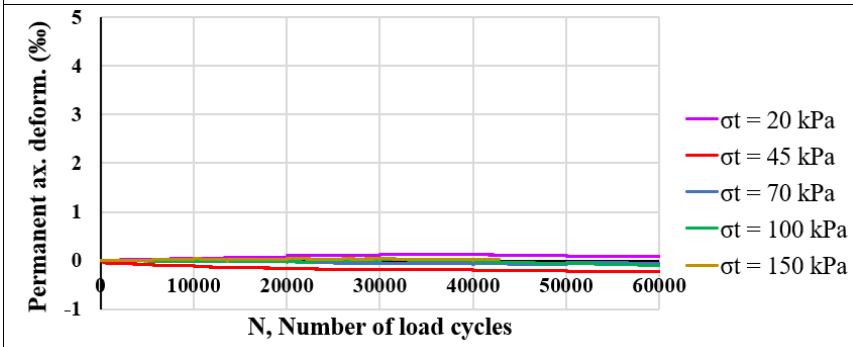

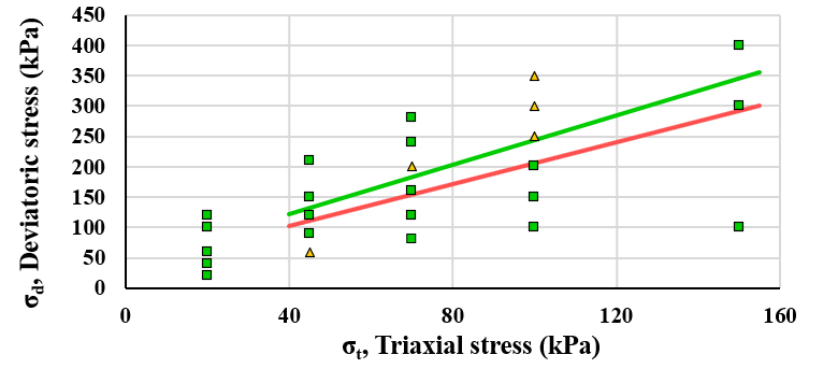

B.10 M2_05 supplementary RLTT data

Sample	M2_05
Water content, *w*	1 %
Additive	-

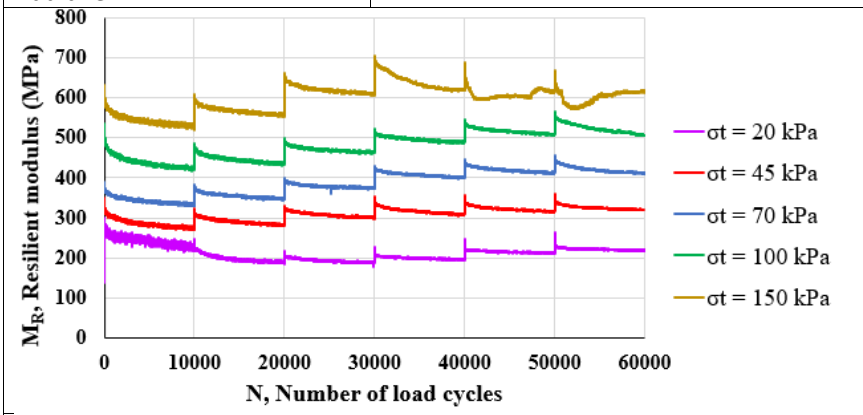

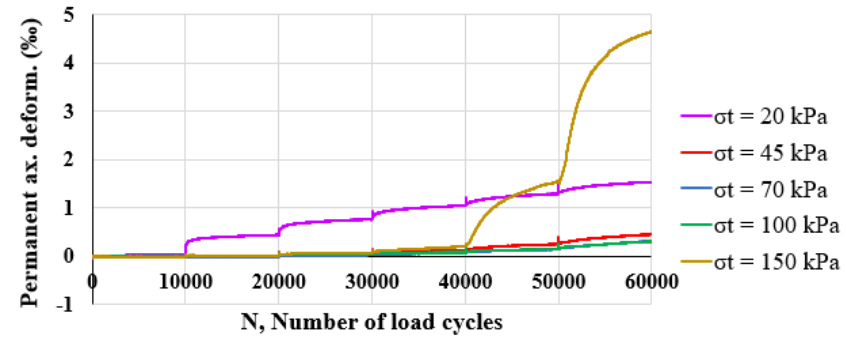

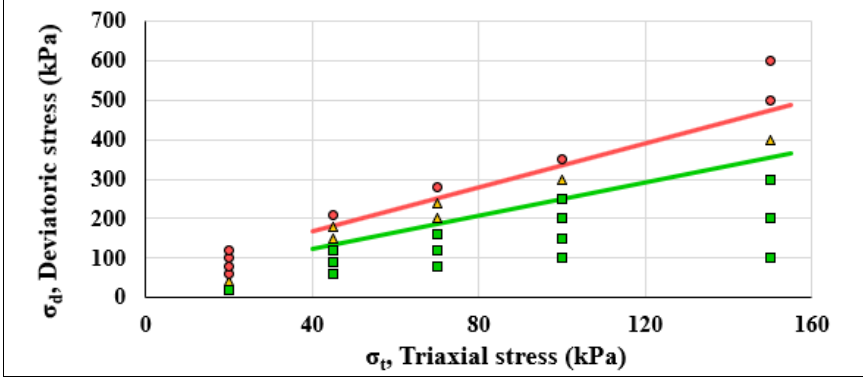

B.11 M2_06 supplementary RLTT data

Sample	M2_06
Water content, *w*	1 %
Additive	-

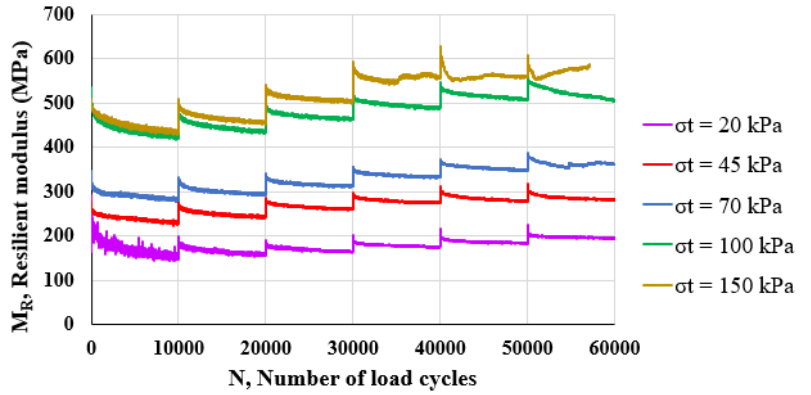

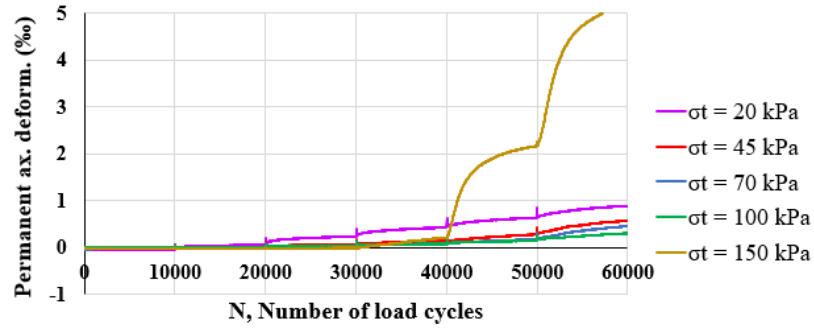

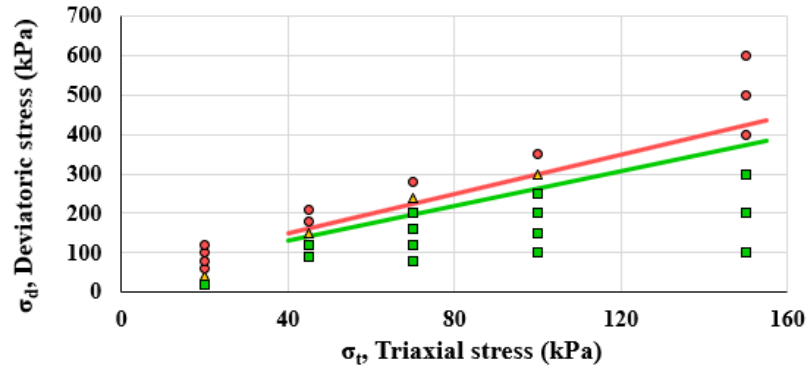

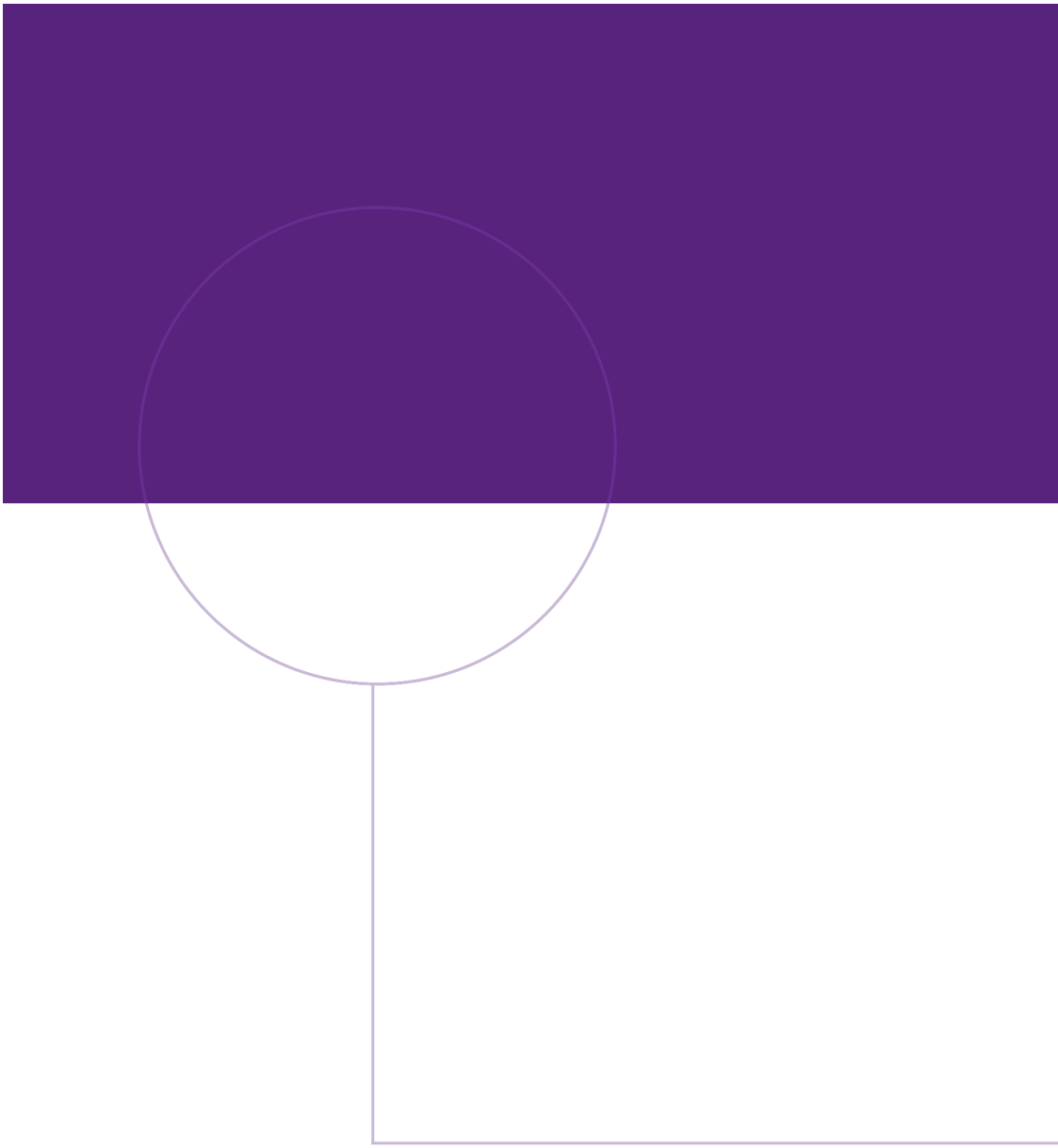

NTNU

Norwegian University of
Science and Technology